Fire Safety Journal 141 (2023) 103922

Contents lists available at ScienceDirect

Fire Safety Journal

journal homepage: www.elsevier.com/locate/firesaf

Fire resistance of gypsum-sheathed stud walls with an embedded steel door: Validation of a numerical approach

Rene Prieler [a,*], Benjamin Ortner [a], Thomas Pfeifer [a], Peter Kitzmüller [b], Stefan Thumser [b], Günther Schwabegger [b], Christoph Hochenauer [a]

[a] Graz University of Technology, Institute of Thermal Engineering, Inffeldgasse 25/B, 8010 Graz, Austria
[b] IBS-Institut für Brandschutztechnik und Sicherheitsforschung GmbH, Petzoldstraße 45, 4020 Linz, Austria

ARTICLE INFO

Keywords:
Gypsum
Stud wall
Fire resistance test
Thermo-mechanical analysis
Finite element modelling

ABSTRACT

In the present study fire resistance tests of gypsum-sheathed stud walls were carried out and a fire safety steel door was embedded within the wall to address the mechanical interaction in between. A numerical approach was proposed based on coupled computational fluid dynamics/finite element method simulations to predict the temperatures and deformation. Since the heat transfer within the porous materials of the wall is crucial for the structural analysis, the numerical approach considered the conduction, chemical reactions, water vapour transport/phase change and thermal radiation. This detailed consideration showed good agreement to measured data for the wall and the door. It was highlighted, that the deformation of the door was well predicted, however, in the vicinity of the connections between the door and wall (e.g. door lock and bolts), the deformation was under-predicted. This was caused by the damaged connections, which were not considered in the simulation. The same effect was found for the wall. Although the numerical model was able to calculate the deformation behaviour, the predicted values were under-predicted due to the neglected failure of the gypsum boards. Furthermore, the numerical model was able to show the gap formation between the door and the wall with high accuracy.

1. Introduction

In modern civil engineering the development of fire safety strategies is still in progress and have led to significant advances in fire protection and safety. Testing real fire scenarios on a large-scale level is related to high efforts for preparing the experimental setup and carrying out the fire tests. However, such experiments with its measured data (temperature, heat fluxes or deformation/displacement) can provide a detailed look on how a fire develops/spreads and its effect on the building components or other structures in civil engineering. This knowledge is essential to avoid fire incidents, such as the travelling fire in the twin towers of the World Trade Centre [1] or the Windsor Tower in Madrid [2] as well as further improve fire safety measures. In 2017, Dai et al. [3] stated in their review paper that there is still a lack of knowledge regarding the physical mechanisms behind the travelling fire, or how a fire spreads in compartments/buildings. As a consequence, Dai et al. proposed a travelling fire framework, which showed that available data in literature is insufficient for model development. Thus, the experimental work on large-scale fire tests considering the fire spread was extended by many researchers in the recent years (e.g. [4] and Nadjai et al. [5] in the course of the TRAFIR project supported by the European Union). The experiments were often supported by numerical simulations predicting the fire spread in the compartments (e.g. Li et al. [6] and Nan et al. [7]). Due to the increasing computational power in the last years, researchers were able to simulate travelling fires in multi-story steel-framed structures and predict the overall robustness in the case of a fire event (e.g. Martinez and Jeffers [8], Shan and Pan [9]). There are a lot more publications to be mentioned in this context, but not considered in this manuscript.

The main task of the aforementioned studies is to identify the fire spread as well as the time-dependent temperature of the fire within a structure consisting of many compartments (or temperature distribution in the compartments in general). Due to the different boundary (e.g. ventilation) or initial conditions (e.g. type of fuel or material which is burning), the fire event can be very complex. Furthermore, the spreading rate of a travelling fire within a building is also affected by the walls (including the fixtures within the walls) separating the compartments. The fire resistance of a wall construction and its fixtures, such as doors, windows etc., is essential to prevent/reduce the fire spread and should give people enough time to be evacuated from a burning building without coming into contact with the hot gases/smoke

* Corresponding author.
E-mail address: rene.prieler@tugraz.at (R. Prieler).

https://doi.org/10.1016/j.firesaf.2023.103922
Received 19 March 2023; Received in revised form 2 June 2023; Accepted 19 August 2023
Available online 21 August 2023

from the fire source. This means that fixtures within the walls as well as the wall itself need to be able to withstand the fire with regard to its thermal resistance, leakage of the hot gases/smoke and structural integrity within a certain time period. However, the fire development in a large-scale multi-story building is affected by many issues (boundary and initial conditions), thus, the correct determination of the fire resistance of a wall with its fixtures is difficult. This is even more critical, when the fixtures are part of a fire safety strategy to prevent a certain compartment to be burnt (e.g. emergency exits, storage for chemicals or explosive materials). Since many full large-scale fire tests to determine the fire resistance of walls and its fixtures (e.g. doors) under various initial and boundary conditions are cost and time consuming, they cannot be carried out for each fire safety equipment. Thus, a reduced standard procedure was introduced (standard fire resistance test). Although standard fire resistance tests (FRTs) cannot represent a real fire scenario, it was established as a classification and certification method for fire safety equipment. According to Downer [10] (*Since even the most 'realistic' tests will always differ in some respects from the 'real thing', engineers must determine which differences are 'significant' and which are trivial if they are to know that a test is relevant or representative.*) it has to be defined which initial and boundary conditions represent the real fire accurately during a standard FRT. For this purpose, it was assumed that a certain (pre-defined) time-dependent temperature trend of the hot gases in the vicinity of the tested fire safety equipment can be used as approximation of a real fire. This time-dependent temperature trend has its basis on fire tests at the beginning of the 1900s (see [11]) and can be found in the standard [12].

1.1. Standardized fire resistance test (FRT)

It was examined above that a standard FRT cannot represent a real fire scenario within a building caused by the various initial and boundary conditions affecting the temperature, smoke development and spreading rate of the fire. Nevertheless, FRTs are still used to test smaller structures, such as fire safety equipment (doors, windows etc.) and walls, when they are exposed to the pre-defined temperature trend (standard fire). These tests are not about the robustness of an entire building but rather the time a fire safety equipment can prevent the fire reaching the next compartment or room within a building. To carry out standard FRTs according to [12], a furnace operated with several burners (oil or gas fired) has to be used. The front side of this furnace is not covered by a wall. Instead, a frame with a certain wall construction is placed on this free side, where the fire safety equipment (test specimen) has to be embedded. The wall can be made of bricks, stud wall or other materials and it is also exposed to the hot gases in the test furnace, heated up and deformed by the thermal exposure. In the furnace, several thermocouples are placed approx. 100 mm away from the tested wall construction to record the gas temperature inside and maintain the pre-defined temperature trend by adapting the burner's fuel input. In that way, the test specimen's (fire safety equipment) thermal resistance (1) and structural integrity (2) against a standard fire can be examined. The behaviour of the wall construction under fire exposure is also an essential issue in standard FRTs. This is caused by the deformation during the heating process, which is completely different from the deformation of the test specimen. Therefore, a gap formation between the test specimen and the adjacent wall construction can be observed. The gap formation is increasing the risk of flue gas leakage from the furnace, which is equivalent to the smoke leakage and fire spread to the next compartment in a real fire scenario. Thus, according to the standard [12], the FRT is used to determine the time period a test specimen within a wall construction can resist a standard fire addressing (1), (2) as well as the prevention of flue gas/smoke leakage to the next compartment (3). As a consequence, manufacturers of doors, windows etc. rely on FRTs, where their products can be tested in conjunction with various wall constructions.

1.2. Numerical modelling of fire events and standard FRTs

Although FRTs are a simplified consideration of real fire scenarios within entire buildings, they are still cost and time consuming to carry out due to the preparation of the test setup, execution and data analysis. Therefore, numerical simulations are getting more attention in fire safety engineering to increase the detailed knowledge of what is going on during a fire event. The numerical methodology has to take into account the (i) combustion process (fire) and heat transfer in the gas phase, (ii) the heat transfer within the solids (steel construction or fire safety equipment) and (iii) deformation process as well as their interactions (see Welch et al. [13] and Tondini et al. [14]). Considering all effects is leading to a complex methodology and is not described before in literature. However, simplifications were regularly used in the past by many researchers to predict standard fires as well as travelling fires numerically (see Section 1). The easiest way is to consider the gas phase combustion (fire) without the heat transfer in the solids and their deformation (e.g. Welch and Rubini [15]). Other researchers used the pre-defined temperature (standard fire) as boundary condition to calculate the heat transfer through the solid test specimen during FRTs (e.g. Ghazi Wakili et al. [16], Hugi et al. [17]). Simulation of the combustion process (fire) and the heat transfer within the solids (test specimen) were commonly done by coupled CFD/FEM (computational fluid dynamics/finite element method) simulations (e.g. [18,19]). Another option is to solve the conjugate heat transfer problem at the fluid/solid interface completely in a CFD code as shown by Kolaitis et al. [20,21] and Prieler et al. [22,23]. They presented a methodology, which allows the consideration of the conjugate heat transfer and the mass transfer between the solid and the fluid side (fire side) including the effect on the temperature of the fire. In Fig. 1 the interaction between the fluid phase and the solid test specimen is marked by the black line. In FRTs also the deformation process of the test specimen as well as the deformation of columns etc. in buildings is of high interest. Therefore, the methodology in Fig. 1 can be extended (see blue line/arrow), which can be referred as *one-way* coupling or *weak coupling*. CFD simulations are commonly used to predict the heat transfer to the solids. Subsequently, the heat transfer and structural analysis is carried out by FEM simulations simultaneously (e.g. [24–27]). Prieler et al. [28] proposed a methodology, where the conjugate heat transfer and temperature in the solid were calculated by CFD simulations. A mapping procedure was applied for the local and temporal temperature distribution in a test specimen during a FRT, and, subsequently, a structural analysis was carried out. The deformation or destruction of solid parts exposed to a fire can affect the gas phase combustion and flame spread in a building significantly (see red lines/arrows in Fig. 1). Whereas experiments are carried out in the past, numerical procedures considering the effect of the structural performance on the combustion are sparse (denoted as *two-way* or *strong* coupling). Feenstra et al. [29] proposed a two-way coupling procedure, where the failure/destruction of panels in an office room due to a fire was investigated. Based on the predicted failure the CFD simulation domain was changed to take the additional ventilation into account. Furthermore, in FRTs often the deformation of the test specimen can lead to gaps between the test specimen and the adjacent wall. Prieler et al. [30] presented a methodology, to predict the gap formation between a fire safety steel door and the adjacent wall during a FRT using coupled CFD/FEM simulations. However, the wall construction was considered as stiff and was not deformed in the model, which is a major drawback for an accurate prediction of the flue gas leakage and fire/smoke development within a building. It can be seen that numerical approaches are available to predict the fire resistance of fire safety products or walls when they are exposed to standard or real fire scenarios on compartment level. However, the methods from Feenstra et al. [29] and Prieler et al. [28,30] considered the behaviour of the solid test specimen without interaction with its neighbouring parts/walls, which can affect the overall deformation significantly. For example, Prieler

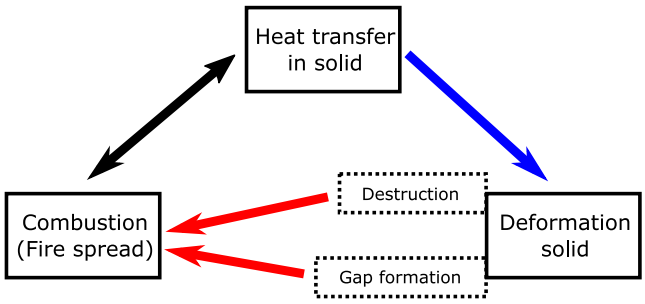

Fig. 1. State-of the-art methodology for the simulation of FRTs/fire events.

et al. [31,32] carried out an experimental study of the wall deformation during FRTs with embedded fire safety steel doors. It was found that the size and type of door is highly affecting the deformation of the wall, which is leading to a different gap formation between the steel door and the wall. Therefore, the structural interaction of the solids exposed to a fire source should be considered in numerical models. So, for the accurate prediction of the fire spread as a result of gap formation and destruction of solid parts, a solid/solid interaction is inevitable. This is also suggested in [28].

In the study of Prieler et al. [28], the numerical approach to carry out the thermal and structural analysis of steel doors, which was also used in the present study, was proposed. The results showed that the maximum deformation of the door was under-predicted. It was concluded that the neglected thermal and structural analysis of the adjacent wall construction was the reason behind the deviation between simulation and measurement. Although a simplified two-way coupling approach was presented in Prieler et al. [30], the result of the predicted door deformation in the vicinity of the door edges/wall still showed a higher deviation compared to the measurement. Therefore, Prieler et al. started an experimental campaign in [31,32] to show the effect of the steel door on the deformation of the wall. Based on these results, the authors started to develop a numerical methodology to enhance the model from [28] by ...

- ... implementing a thermal model considering the heat conduction, chemical reactions, water vapour transport/phase change and thermal radiation in the stud wall,
- determining accurate contact treatments between the door and the wall in order to predict the mechanical interaction as well as the gap formation and
- experimentally investigating the stress–strain curves of gypsum at elevated temperatures.

The experimental data for the FRTs used in the present study were derived from Prieler et al. [31].

2. Stud walls under fire exposure and objectives of the present study

2.1. Review — experimental and numerical investigations of stud walls

In this section the fire-related consideration of stud walls published in recent years will be examined briefly. A study carried out by Dias et al. [33] investigated gypsum- and steel-sheathed stud walls using standard fire conditions. They found out that the temperature of the studs are similar in both cases. However, Pancheti and Mahendran [34] used autoclaved aerated concrete (AAC) to cover the studs, which enhanced the fire resistance of the wall compared to the gypsum-sheathed setup. Furthermore, Gnanachelvam et al. [35] tested phase change material (PCM) cellulose insulation on the stud wall, which was leading to a better thermal resistance, and subsequently improved the fire performance. Not only the cover type of the studs is affecting the fire resistance of the wall, but also the steel type and profile which are used for the studs. Ariyanayagam and Mahendran [36] showed that the fire resistance decreased by approx. 25% when the studs were made of low strength steel. In another study Tao et al. [37] applied hollow section steel studs instead of conventionally used steel profiles within the wall. Although an increased heat transfer from the fire side to the fire unexposed side was observed, the temperature gradients in the studs were lower, which reduced the thermal bowing of the studs. As mentioned in Section 1, the *real* fire resistance also depends on the fire scenario, which was the main focus in the work of Chen et al. [38,39]. In addition to the mentioned experimental studies, researchers also used numerical simulations to determine the temperatures in the stud walls and the deformation caused by the thermal exposure (e.g. Nassif et al. [40], Ye and Chen [41], Yu et al. [42], Abeysiriwardena and Mahendran [43]). It has to be mentioned that these studies, investigating stud walls under fire exposure, were done without fixtures (wall only). However, Prieler et al. determined in a recent study that the type of fixture as well as its size are affecting the stud wall's deformation significantly [32]. There is just one additional study, which reported the fire performance of a stud wall with an embedded fire safety steel door from Nassif et al. [44]. The different thermal expansion behaviour of the wall and its fixtures is leading to a mechanical interaction and was not investigated in the past, although this effect might be crucial for the gap formation, and subsequently flue gas and fire spread from one compartment to the next one. Furthermore, the numerical studies by Nassif et al. [40] as well as Abeysiriwardena and Mahendran [43] only simulated the deformation of a single steel stud in the wall, which might be accurate enough when the considered stud is in the middle of the wall. However, near the wall's edge the deformation is clearly different (see Nassif et al. [40]). This is the same when the steel stud is near a fixture in the wall. There was also no effect of the connecting gypsum boards on the deformation behaviour taken into account. In contrast, Ye and Chen [41] tried to compensate the presence of the gypsum boards by applying appropriate boundary conditions at the connections between the steel studs and gypsum boards. Nevertheless, there is still no numerical study available, which also contains the effect of the gypsum boards on the deformation process of the studs as well as the entire wall, respectively.

2.2. Objectives of the present study

In the present study a fire safety steel door was embedded within a gypsum-sheathed stud wall , which will be exposed to standard fire conditions according to [12]. Three FRTs were carried out with different positions of the steel door within the stud wall. For each FRT the temperatures in the furnace (gas temperature), the temperatures at the fire unexposed side as well as the deformation of the wall and the steel door (also denoted as test specimen in this study) were observed. Furthermore, the gap formation between the steel door and the adjacent stud wall will be determined, qualitatively. Subsequently, the experimental results were used for the validation of the numerical model.

The numerical methodology, which is the main focus of the study, is based on the work of Prieler et al. [28] and was already tested to calculate the temperatures and deformation of fire safety steel doors. It was suggested by Prieler et al. that the simulation should also include the deformation of the wall construction to enhance the quality of the predicted data. Besides the calculation of the temperatures within the solids (wall + test specimen), the methodology was adapted to also consider the structural interaction between the steel door and the stud wall to predict the gap formation during the FRT (see Fig. 2). So, the objectives of this study can be summarized:

- Calculation of the heat transfer in the gypsum-sheathed stud wall including the heat conduction, mass transfer of water vapour, condensation and evaporation as well as the radiative heat transfer.

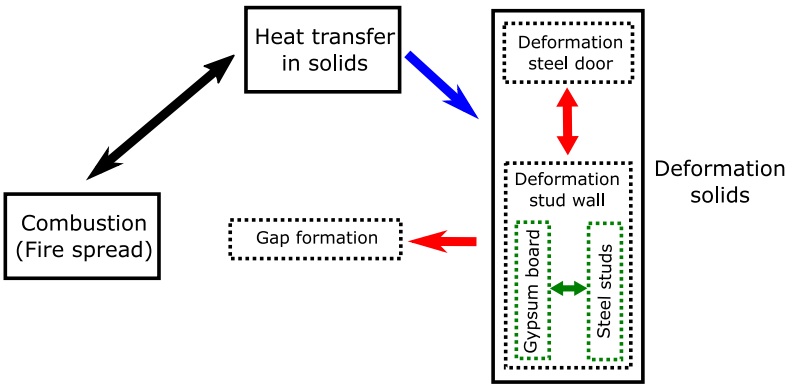

Fig. 2. Methodology for the simulation of FRTs/fire events including the structural interactions between solid parts (wall and test specimen).

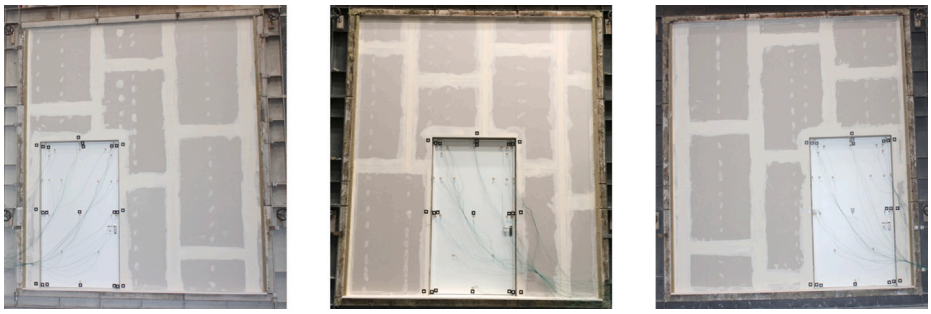

Fig. 3. Three test configurations for the steel door within the gypsum-sheathed stud wall: Door in left position (denoted as *DL*), door in central position (denoted as *DC*) and door in right position (denoted as *DR*).

- Modelling approach for contact faces between the wall and the steel door (fixed connections and sliding faces).
- Simulation of the deformation process and the interaction of the wall and test specimen during the FRT. The mechanical analysis will involve the mechanical behaviour of the gypsum boards and the results will be compared to the measured data.
- Determination of the gap formation between the steel door and the wall due to the deformation process and their interactions.

3. Experimental setup and material properties

In this study three FRTs were carried out, where a fire safety steel door was used as test specimen. The door was embedded in a gypsum-sheathed stud wall and the experimental data were used to validate the simulation methodology. To highlight the capability of the numerical approach, three test configurations were applied, which can be seen in Fig. 3. Since it was found in [31] that also the position of the test specimen is changing the deformation behaviour of the stud wall, the placement of the door is different. This should increase the validity of the numerical model.

3.1. Fire resistance test furnace

The entire construction (wall + test specimen) was placed at a fire resistance testing furnace with its dimension of 4000 × 4500 × 1250 mm (see Fig. 4). It was equipped with four natural gas fired burners (Eclipse ThermJet TJ300BHN-BX), with baffle sheets in front of the burners to deflect the flames and ensure a more homogeneous temperature distribution in the furnace (see [45]). A control system adapted the fuel input during the FRTs to ensure that the gas temperature in the furnace is in close accordance to the standard fire conditions based on [12] during the entire testing time of 30 min. The gas temperature in the furnace was observed by 12 plate thermocouples, which are placed

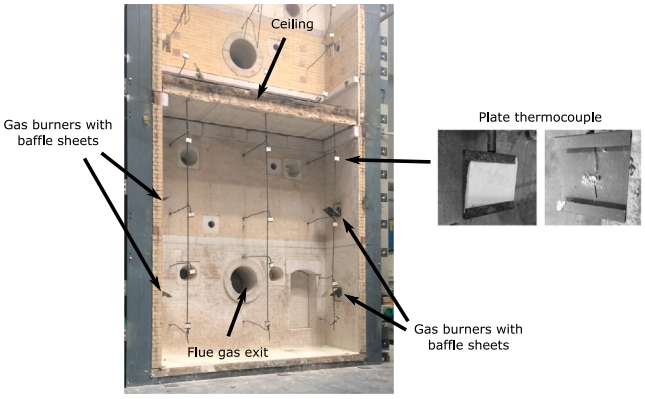

Fig. 4. Fire resistance test furnace without wall construction and test specimen at the front.

approx. 100 mm from the test specimen/stud wall. The walls of the furnace were a multi-layer construction made of fire bricks and ceramic insulation, whereas the ceiling was formed by fibre insulation panels (thickness: 345 mm and 230 mm).

3.2. Gypsum-sheathed stud wall

As it can be seen in Fig. 3, the FRT was carried out for a fire safety steel door embedded within a gypsum-sheathed stud wall, which can be seen in Fig. 5. In the wall CW-shaped steel profiles (100 × 50 × 0.6 mm) were vertically arranged. The distance between the CW-shaped vertical steel studs was 625 mm. Around the steel door, UA-shaped steel profiles (100 × 40 × 2 mm) were placed in addition to the CW-shaped studs. At both sides (fire exposed and unexposed) two gypsum boards (thickness of 12.5 mm per board) were fixed at the studs and the void in between

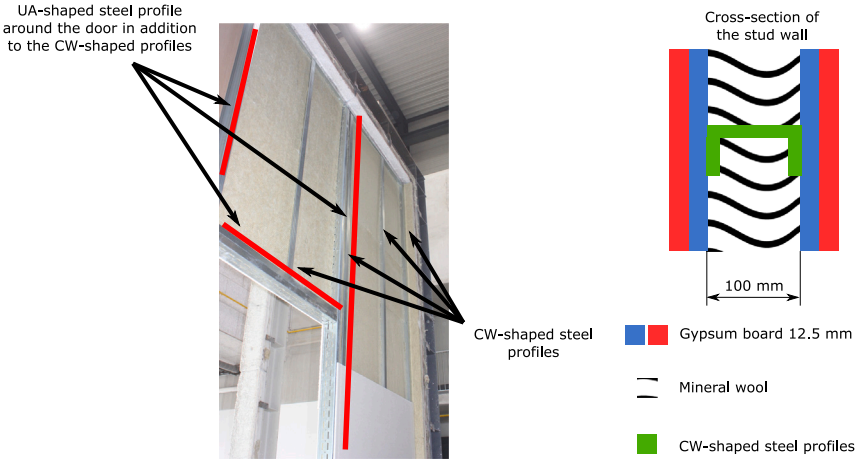

Fig. 5. Setup of the gypsum-sheathed stud walls.

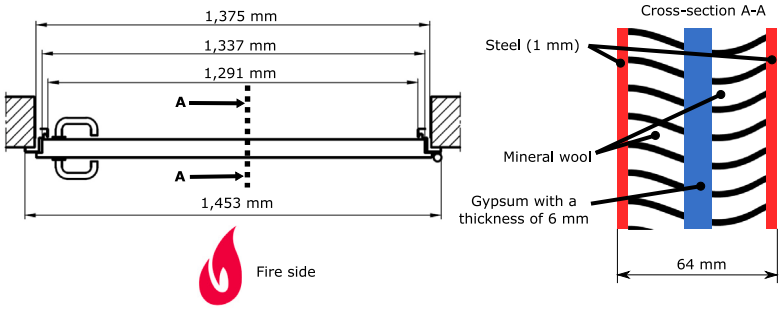

Fig. 6. Inner construction of the fire safety steel door.

was filled with mineral wool (see Fig. 5). For the test cases *DL* and *DR* the door was placed in a distance of 200 mm from the left and right edge of the wall, respectively. At the wall, several measurement points were fixed to observe the deformation of the wall during the FRT (see Section 3.3).

3.3. Test specimen — Fire safety steel door

In all three FRTs the same door type was used. In Fig. 6 the width of the door is presented. The building dimension width was 1375 mm and its corresponding height was 2500 mm, whereas the leaf dimension width was 1337 mm and the height was 2475 mm. Furthermore, the hinges of the door were exposed the fire side. The steel casing of the door was made of sheet metal with a thickness of 1 mm. To enhance the fire resistance of the door, a gypsum board was placed in the middle of the cross-section with a thickness of 6 mm. The void between the steel and gypsum was filled with mineral wool, leading to an entire thickness of the door of 64 mm.

The door's frame was fixed with the wall at several positions, which are highlighted in Fig. 7 (left and centre) by the black dashed boxes. All connections were also considered in the FEM simulation in this study. Furthermore, when the door is closed, there are several connections between the door and the door's frame. At the side of the door lock, there is only one connection at the height of the door lock. At the other edge of the door three security bolts are snapped into the frame over the entire height of the door when the door is closed (see red dashed box in Fig. 7). In addition, the door is connected to the frame by two hinges, also presented in 7 (red dashed box). All mentioned connections are considered as fixed in the following numerical model.

3.4. Material properties

In this subsection the material properties for steel, gypsum and mineral wool, which are needed for the following CFD and FEM simulations, are presented.

3.4.1. Steel

The thermal properties of the steel studs for the numerical simulations in this study were chosen from the work of Nassif et al. [40], which were derived from the Eurocode 3 [46]. This includes the temperature-dependent specific heat capacity as well as the thermal conductivity. Furthermore, the density of steel was set to 7850 $\mathrm{kg/m^3}$. Although the thermal properties were not determined by the authors for the same steel type used for the studs, the data from Eurocode 3 were successfully used in the past for the thermal analysis (e.g. Nassif et al. [40]). For the structural analysis also the temperature-dependent thermal expansion and mechanical properties of the steel are essential. The thermal expansion coefficient and the Poisson ratio were used based on Ref. [28]. The stress–strain curves were determined based on the model proposed by Luecke et al. [47]. However, the model coefficients from Zhang et al. [25] were used in the model to calculate the temperature-dependent elastic modulus and the stress–strain curve, which can be seen in Table 1 and Fig. 8 for a number of temperature levels. The model of Luecke et al. [47] was used in this study to predict the stress–strain behaviour at high temperature, because Luecke et al. determined that it calculates the stress–strain behaviour of steel slightly better than the Eurocode 3 [46]. A further improvement of the model from Luecke et al. can be achieved by using the model coefficients from Zhang et al. [25]. The mechanical properties as well as the calculation methods are also summarized in Prieler et al. [28].

3.4.2. Gypsum

Nassif et al. [40] also presented temperature-dependent thermal properties of gypsum boards (density, specific heat capacity and thermal conductivity) in their study, which were also used for the thermal analysis here. Thus, the same properties were applied in the simulations. Since gypsum mainly consists of calcium sulphate di-hydrate ($CaSO_4 \cdot 2H_2O$), water vapour will be released from the porous gypsum during the heating process. It was found by Prieler et al. [48] that the water vapour can be transported within the porous structure of

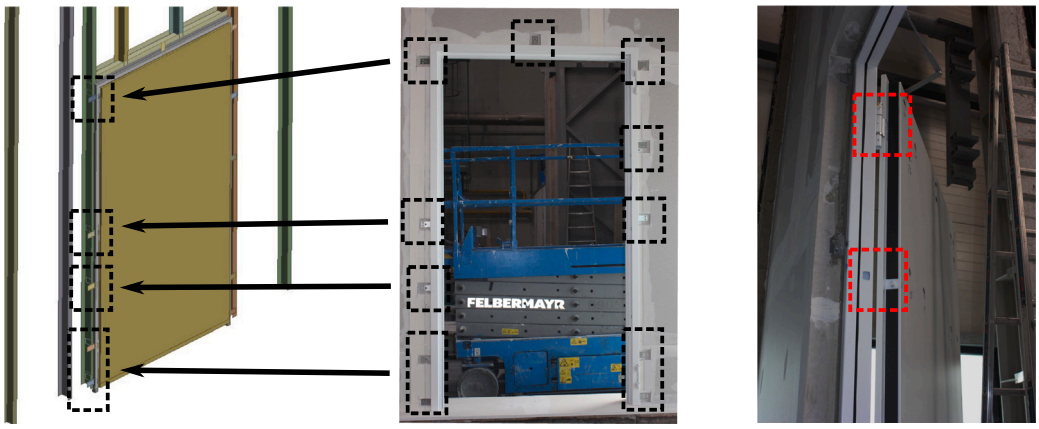

Fig. 7. Fixed connections between the door's frame and the wall as well as the door leaf and the door's frame.

Table 1
Temperature-dependent elastic modulus of steel.

Temperature [°C]	Elastic modulus [$\times 10^6$ Pa]
20	215,000
50	213,053
100	209,809
200	202,729
300	193,150
400	178,563
500	156,814
600	127,459

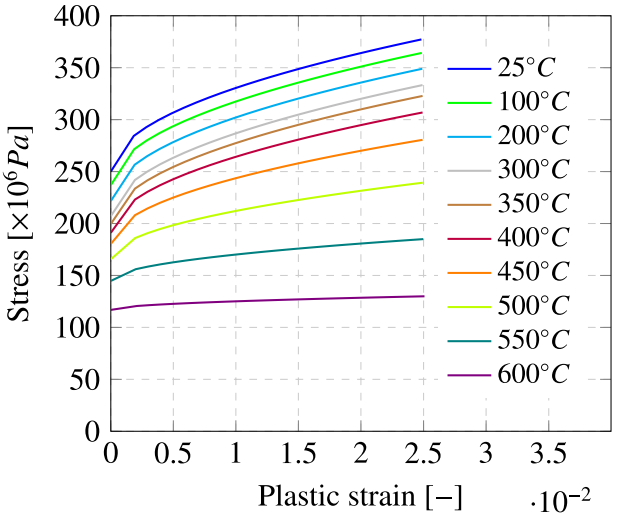

Fig. 8. Temperature-dependent stress–strain curves for steel.

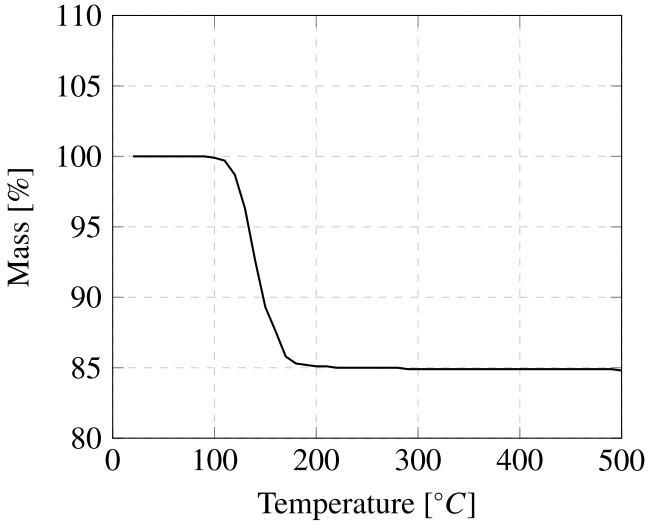

Fig. 9. Mass loss of gypsum during the heating process [50].

the gypsum and the mineral wool, and represents a key phenomenon regarding the temperature trend in multi-layer gypsum/mineral wool constructions. Due to the transport within the porous structure, the water vapour can reach colder regions inside the gypsum/mineral wool of the stud wall and condenses there. As a consequence, heat will be released locally, which heats up the solid material much faster. The condensed water keeps the solid material at a constant temperature level of about 100 °C until the re-evaporation is finished, based on the further heating from the fire side. It was suggested by Weber [49] and Prieler et al. [50] to include the mass transfer of water vapour as well as the condensation and evaporation effects into the numerical model. For this purpose, a temperature-dependent mass source term for the water vapour within the porous gypsum boards have to be determined and used in the transport equations (see Section 4.1.2). The source term is based on the measured mass loss of gypsum during the heating process, which can be seen in Fig. 9. It can be seen that the mass loss (water vapour release within the porous gypsum) occurs between 110 and 180 °C. This is in close accordance to the peak value of the specific heat capacity of gypsum shown in Nassif et al. [40], indicating the chemical reactions causing the water vapour release.

In contrast to other studies numerically considering the fire-induced deformation of the steel studs within the wall, the present study also involves the mechanical behaviour of the gypsum boards when they are attached to the steel studs during the fire. Due to the thermal bowing of the steel studs, the gypsum boards attached to the studs are deforming too. Thus, the mechanical properties were examined by three-point flexural tests of the gypsum samples at different temperature levels. In these tests the gypsum sample is placed on two support points and a mechanical load is performed on the sample between these points. Subsequently, the gypsum sample is exposed to a bowing deformation. The test setup can be seen in Fig. 10, which was carried out with a *Zwick Z005* machine embedded in a *Linn High Term* furnace.

To carry out the flexural tests, gypsum samples with the dimension of 12.5 × 22.4 × 170 mm were cut from the gypsum boards. The distance between the support points was 150 mm. Before the test, the furnace was heated up to a certain temperature level, besides the test at ambient temperature (approx. 25 °C), which was 200, 400, 600 and 750 °C. When the temperature level was reached, the sample was placed at the supporting points. A residence time of 5 min

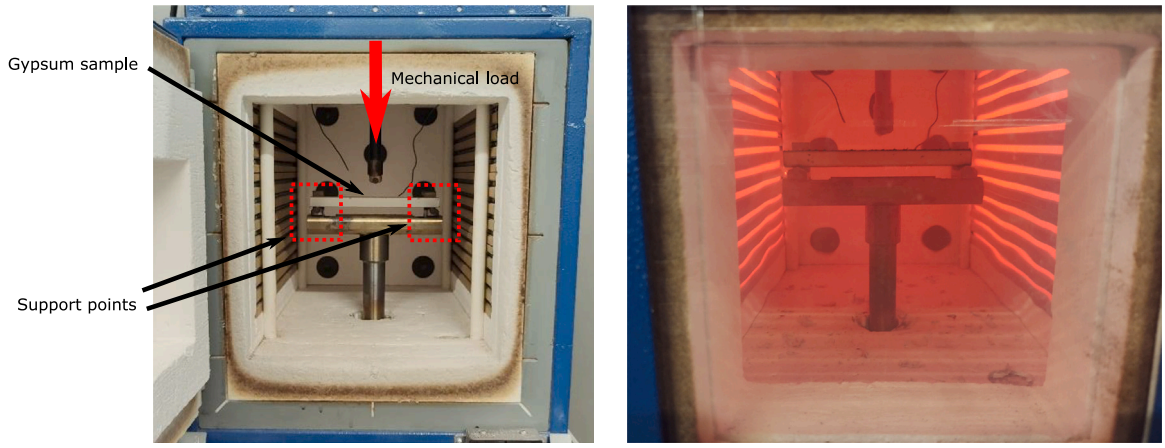

Fig. 10. Three-point flexural test of gypsum samples: Before the test (left) and at a temperature level of 750 °C (right).

Table 2
Temperature-dependent elastic modulus of gypsum based on the flexural tests.

Temperature [°C]	Elastic modulus [$\times 10^6$ Pa]
25	2,210.5
200	1,210.5
400	178.0
600	97.0
750	12.3

was chosen before the mechanical load was applied. This time was considered as sufficient to ensure that the gypsum sample is heated up to the temperature level homogeneously. For each temperature level two experiments were carried out and the average values were calculated and further used in this study. In Fig. 11 the measured flexural stresses are shown for each temperature level. At low temperatures up to 200 °C the stresses linearly increase with the deformation of the sample until its peak values of 307 × 10^4 Pa and 197 × 10^4 Pa at approx. 0.45 mm, respectively. A second stress peak can be observed until the flexural stress is significantly decreasing. At a temperature level of 400 °C the maximum flexural stress is lower compared to ambient temperature and 200 °C. Also the increase of the stress at the beginning is a little bit more curvy, but can also be approximated as a linear function. The maximum stress was determined at 0.79 mm with a value of 95 × 10^4 Pa. At 600 and 750 °C the maximum flexural stress was approx. 15 × 10^4 Pa. It has to be mentioned that after the maximum peak stress was reached cracks in the gypsum sample were observed optically. Thus, at this point it is unclear how the cracks are affecting the structural integrity of the gypsum boards as well as the connectivity between the gypsum board and the steel studs during the FRT. Therefore, the data from the flexural tests cannot be used for the prediction of the gypsum board failure. Thus, for the structural analysis of the wall, only the data from the linear increase of the flexural stress to its peak value will be used, since the structural integrity of the board in this range is ensured. Assuming a linear stress–strain trend to the maximum peak stress, the elastic modulus can be determined (see Table 2). It has to be noted, that the structural integrity of the gypsum boards will be over-estimated in the numerical simulations with these assumptions and fall-off cannot be simulated, which will increase the mechanical stability of the wall. Thus, it is expected that the structural analysis of the stud wall will lead to a lower deformation compared to the experiment.

3.4.3. Mineral wool

For the mineral wool the density was fixed with a value of 25 kg/m^3. Furthermore, the specific heat capacity and thermal conductivity was

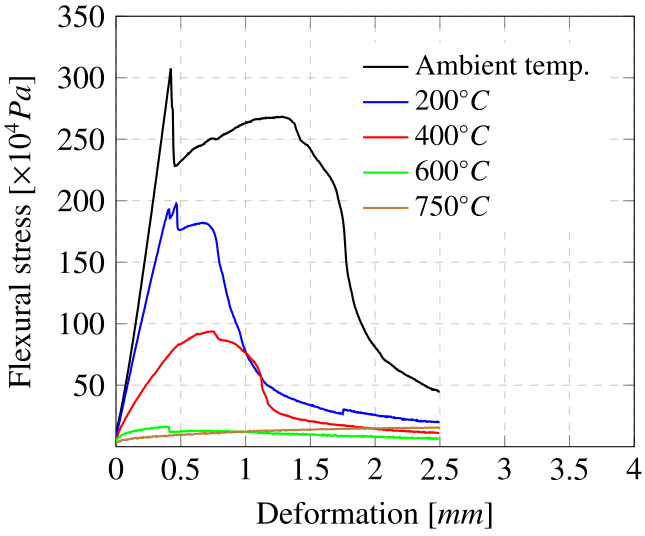

Fig. 11. Measured flexural stress and deformation of the gypsum sample at ambient temperature, 200 °C, 400 °C, 600 °C and 750 °C.

set to values of 840 J/(kg ∗ K) and 0.035 W/(m ∗ K), respectively. These values are based on the data sheet from the supplier and are in accordance to the data shown in Nassif et al. [40]. For the structural analysis it was assumed that the contribution of the mineral wool to the deformation process is low. Furthermore, there is also a lack of published mechanical data for mineral wool at higher temperature levels, which would be needed for the simulations in this study. Therefore, mechanical data were not considered for mineral wool.

4. Numerical methodology

In this section the numerical methodology will be described, which is based on the work of Prieler et al. [23,28]. The CFD/FEM coupling approach by Prieler et al. showed its capability to predict the gas phase combustion and heat transfer in solids as well as their interactions regarding the heat fluxes and mass transfer. Furthermore, the deformation of the solid test specimen can be calculated. However, it was highlighted in Section 1 that also the deformation of the adjacent wall construction has to be considered. Therefore, the deformation process will not be limited to the test specimen in the present study and the numerical methodology from Prieler et al. was enhanced to address the following points in addition to the basic methodology:

- Prediction of the heat transfer within the porous structure of gypsum and mineral wool with regard to the water vapour transport (released by gypsum), partial condensation and evaporation as well as the radiative heat transfer in addition to the basic heat conduction.
- Deformation of the steel studs and gypsum boards (fixed connection without failure mode) in interaction with the test specimen's (steel door) deformation.
- Determination of the gap formation between the wall and the door, and comparison with the experimental observations.

It has to be mentioned that the methodology of Prieler et al. [23,28] also includes the gas phase combustion, which allows a spatial and temporal resolution of the heat fluxes between the fire and the solids (wall/test specimen). Since the focus was the modelling of the deformation processes and gap formation, the simulation of the gas phase combustion was not done. Instead the thermal boundary conditions at the fire exposed side of the wall/test specimen were derived from the experimental data. Thus, only the heat transfer and structural analysis of the solids were carried out.

4.1. Heat transfer in the wall and test specimen

The heat transfer through the gypsum-sheathed stud wall is affected by the water vapour transport, condensation/evaporation of the water vapour and radiative heat transfer within the porous structure. Prieler et al. [50] presented a numerical methodology to address all these transport phenomena, which is the basis for the heat transfer modelling within the wall in the present study. The simulations will be carried out using CFD (with the finite volume method). Although gypsum was used within the test specimen (steel door), the water vapour transport and condensation/evaporation was not considered for the heat transfer modelling of the steel door. This is based on the numerical instability when the condensation/evaporation model was applied for the steel door. During the phase change of water vapour within the steel enclosure of the door, pressure gradients occur leading to numerical instabilities. First, when water vapour is released from the gypsum the pressure inside the steel enclosure of the door (constant volume) increases. In contrast, when the water vapour is transported to the ambient side, it condenses at the steel enclosure. Subsequently, the pressure is locally decreasing, leading to the mentioned pressure gradient. For this purpose, only the transport equation for the energy without species transport and condensation/evaporation effects was solved (see Section 4.1.2) for the door.

4.1.1. Numerical grid and boundary conditions

For the simulation of the heat transfer through the gypsum-sheathed stud wall, the steel door and the door's frame, a numerical grid for each solid was created. The numerical grid for the stud wall is shown in Fig. 12. Since it can be assumed that the temperature at the fire exposed side during the FRT is homogeneously distributed, the heat transfer model through the wall can be approximated by a reduced computational domain. This reduced computational domain for the wall consists of several sub-domains representing the gypsum boards at ambient and fire side. The green domain in Fig. 12 stands for the mineral wool and the grey zone stands for the steel stud. As already mentioned, the heat transfer through the stud wall is also affected by the water vapour transport within the porous structure, which is released by the gypsum board. This phenomenon was taken into account in the numerical simulation (see Section 4.1.2). To ensure that water vapour can exit the wall, small domains at the fire and ambient side were arranged (see blue and red zone in Fig. 12). When water vapour arrives in these zones it is seen as vanished from the simulation domain. The entire simulation domain for the wall was created by 35,200 hexahedrons with a maximum aspect ratio of 17.7. At the fire side, the domain was defined with the time-dependent average gas temperature in the furnace measured during the FRTs (see Section 5.1). The temperature in the ambient zone was fixed with a value of 25 °C. Both zones (ambient/fire) were defined as pressure-outlets to ensure water vapour can exit the domain. At the ambient side the pressure boundary was chosen in accordance to the ambient pressure. However, during the FRTs a pressure gradient from the bottom to the top of the furnace was observed. Compared to the ambient side a pressure of −1, +4 and 0 Pa (*DC*, *DR* and *DL*) was measured at the bottom of the furnace. Additionally, the pressure at the top of the furnace was +14, +22 and +17 Pa compared to the ambient side. Therefore, an over-pressure of 10 Pa was chosen for the simulation at the fire side. The other boundaries of the domain were defined as adiabatic walls. In Fig. 12 five positions are marked by red dots, where the temperature will be observed and compared to measurements in Section 5.2.

The numerical grid for the steel door consists of approx. 74,500 cells, where the cells for the inner construction of the door (gypsum and mineral wool) are hexahedrons (approx. 12,800 cells). The majority of the cells were used for the steel enclosure of the door. In the enclosure tetrahedrons were used (approx. 61,700 cells) because it made the mesh generation in the region of the door's rebate easier (better quality of the cells). Similar to the steel enclosure of the door, tetrahedrons were also used for the numerical grid of the door's frame, where the number of cells was approx. 66,800.

4.1.2. Multi-phase and species transport modelling in porous structures

Within the porous structure species transport, condensation/evaporation and radiative heat transfer occurs beside the heat conduction. To model these effects the domains for mineral wool and gypsum in the wall (see Fig. 12) were treated as porous zone in the simulation. In the porous domains of mineral wool and gypsum in the wall as well as the ambient and fire zone in Fig. 12, the transport equations for each phase has to be solved in accordance to the Eulerian multi-phase model. In Eq. (1) to Eq. (3) the transport equations for mass, momentum and energy are shown for the q-th phase. In the present case only a gaseous phase (air + water vapour - primary phase) and a liquid phase (condensed water - secondary phase) are present within the porous structure.

$$\frac{\partial(\alpha_q \rho_q)}{\partial t} + \nabla \cdot (\alpha_q \rho_q \vec{v}_q) = \sum_{p=1}^{n} (\dot{m}_{pq} - \dot{m}_{pq}) + \omega_{q_{mass}} \tag{1}$$

$$\frac{\partial(\alpha_q \rho_q \vec{v}_q)}{\partial t} + \nabla \cdot (\alpha_q \rho_q \vec{v}_q \vec{v}_q) = -\alpha_q \nabla p + \nabla \cdot \bar{\bar{\tau}}_q + \sum_{p=1}^{n} (K_{pq}(\vec{v}_p - \vec{v}_q) + \dot{m}_{pq}\vec{v}_{pq} - \dot{m}_{qp}\vec{v}_{qp}) + \omega_{q_{mom}} \tag{2}$$

$$\frac{\partial(\alpha_q \rho_q h_q)}{\partial t} + \nabla \cdot (\alpha_q \rho_q \vec{v}_q h_q) = \alpha_q \frac{\partial p_q}{\partial t} + \bar{\bar{\tau}}_q : \nabla \vec{v}_q - \nabla \cdot (\lambda \nabla T) + \sum_{p=1}^{n} (Q_{pq} + \dot{m}_{pq} h_{pq} - \dot{m}_{pq} h_{qp}) + \omega_{q_{energy}} \tag{3}$$

The variable α_q stands for the volume fraction, $\vec{v}_q$ represents the velocity vector of the qth phase and $\dot{m}_{pq}$ stands for the mass transfer rate from phase q to phase p (see Section 4.1.3). In the momentum equation the p_q represents the pressure and $\bar{\bar{\tau}}_q$ is the stress tensor of the qth phase. Furthermore, K_{pq} is the momentum exchange coefficient, which includes the drag coefficient. To determine K_{pq} the *symmetric* model [51] was used. The phase velocities for the qth and pth phase are represented by $\vec{v}_q$ and $\vec{v}_p$. In addition, the variables $\vec{v}_{pq}$ and $\vec{v}_{qp}$ are the velocities for the mass transfer between the phases. In the energy equation, h_{qp} is the interphase enthalpy and Q_{pq} is the intensity heat exchange between the phases, which was calculated using the Ranz–Marshall model [52,53]. In the transport equations the source terms can be identified by the variables $\omega_{q_{mass}}$, $\omega_{q_{mom}}$ and $\omega_{q_{energy}}$. The source terms in the transport equations are present for the gaseous phase, when water vapour is released from solid gypsum during the heating process. They are temperature-dependent and were derived from the

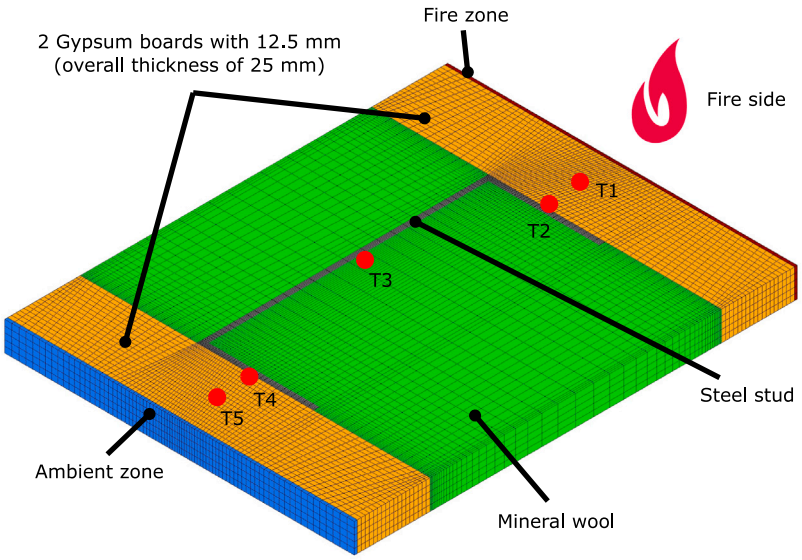

Fig. 12. Numerical grid for the simulation of the heat transfer through the gypsum-sheathed stud wall.

mass loss of the gypsum from Fig. 9. The mass source of water vapour in each cell has the same state as the air (temperature and velocity). As it was mentioned, there is air and water vapour in the primary phase in the simulation. Despite the fact that air mainly consists of nitrogen and oxygen, air was treated as a single component using the properties of air. Since two components are present, a species transport equation for the species i has to be solved within the primary phase (see Eq. (4)). In Eq. (4) $Y_{i,q}$ stands for the mass fraction of species i in the q-th phase (e.g. air in the primary phase). Furthermore, $\vec{J}_{i,q}$ is the diffusion flux of species i and $S_{i,q}$ is the mass source of water vapour released from gypsum during the heating process, which was implemented by a user-defined function (UDF). The term $\alpha_q S_{i,q}$ is equivalent to $\omega_{q_{mass}}$ in Eq. (1).

$$\frac{\partial(\alpha_q \rho_q Y_{i,q})}{\partial t} + \nabla \cdot (\alpha_q \rho_q \vec{v}_q Y_{i,q}) = -\nabla \cdot \alpha_q \vec{J}_{i,q} + \alpha_q S_{i,q} + \sum_{p=1}^{n} (\dot{m}_{p_i q_i} - \dot{m}_{q_i p_i}) \quad (4)$$

The diffusion flux of a species in the q-th phase was calculated according to Eq. (5), where $D_{i,m,q}$ is the mass diffusion coefficient and $D_{T,i,q}$ is the thermal diffusion coefficient (Soret effect) of the species i. It has to be mentioned that the diffusion coefficients in Eq. (5) are temperature-dependent and can be determined by Eq. (6). In Eq. (6) it can be assumed that the pressure in the furnace is similar to the standard conditions ($p_0 = 101,325$ Pa) and the diffusion coefficient at standard conditions D_0 has a value of 1383 mm^2/min for water vapour in air and T_0 is 0 °C (see [48]).

$$\vec{J}_{i,q} = -\rho_q D_{i,m,q} \nabla Y_{i,q} - D_{T,i,q} \frac{\nabla T}{T} \quad (5)$$

$$D(T) = D_0 * \frac{p_0}{p} * \left(\frac{T}{T_0}\right) \quad (6)$$

The diffusion coefficient in Eq. (6) is valid for the diffusion in open space, such as in the fire and ambient region of the wall model in Fig. 12. However, the gypsum and mineral wool in the model were treated as porous zones, where the diffusion process is affected by the pore structure (porosity ϵ and tortuosity τ). Therefore, an effective diffusion coefficient for the porous zones have to be applied, which can be calculated by Eq. (7). Since τ is difficult to determine, manufacturers often publish the water diffusion resistance factor of the material μ_d, which has commonly a value of 10 for gypsum. Although Richter and Stanek [54] measured values around 8.4 and 8.8 for different gypsum plasterboards, the manufacturer's data sheet showed a value of 10, which was then used in this study. For the mineral wool a water vapour diffusion resistance factor of 1.25 was used in accordance to the measurement from Prieler et al. [48].

$$D_{eff}(T) = \frac{\epsilon}{\tau} * D(T) = \frac{1}{\mu_d} * D(T) \quad (7)$$

The mineral wool and the gypsum boards in the wall construction are treated as porous zone in the simulation. That means that not only the diffusion of the water vapour in the structure is slower than in open space (see Eq. (7)), but also the energy equation (Eq. (3)) has to be adapted to take the thermal inertia of the solid mass of the gypsum/mineral wool into account. For this purpose, the transient term on the left hand side of Eq. (3) was changed as shown in Eq. (8). Now, the temporal change of the energy in each numerical cell also considers the energy necessary to heat up the solid material in a numerical cell in addition to the fluid of the q-th phase. The porosity values for gypsum and mineral wool were 0.33 and 0.975, respectively. In the conductive term of Eq. (3) the value for the thermal conductivity now consists of the values for the q-th fluid phase and the solid material (gypsum or mineral wool), as presented in Eq. (9).

$$\frac{\partial(\alpha_q \rho_q h_q)}{\partial t} \rightarrow \frac{\partial(\epsilon \alpha_q \rho_q h_q + (1-\epsilon)\rho_{solid} h_{solid})}{\partial t} \quad (8)$$

$$\lambda = \epsilon \lambda_q + (1-\epsilon)\lambda_{solid} \quad (9)$$

4.1.3. Condensation and evaporation model — Lee model

The condensation and evaporation effects of water vapour within the porous structure of gypsum and mineral wool was considered using the Lee model [55], which was successfully tested for the fire-induced heat transfer in porous gypsum by Prieler et al. [50]. The Lee model calculates the mass transfer rate from the q-th phase to the pth phase $\dot{m}_{qp}$ and vice versa $\dot{m}_{pq}$ as given in Eq. (10) and (11). The saturation temperature was set to a value of 100 °C and is denoted by T_{sat}. The condensation and evaporation frequencies (r_{qp} and r_{pq}) were defined with values of 300 min^{-1}. In Prieler et al. [50] a value of 60 min^{-1} was suggested, however changing the value to 300 min^{-1} was leading to a better agreement to the validation data in Section 5.2.

$$\dot{m}_{qp} = r_{qp} \alpha_q \rho_q \frac{T_q - T_{sat}}{T_{sat}} \quad (10)$$

$$\dot{m}_{pq} = r_{pq} \alpha_p \rho_p \frac{T_{sat} - T_p}{T_{sat}} \quad (11)$$

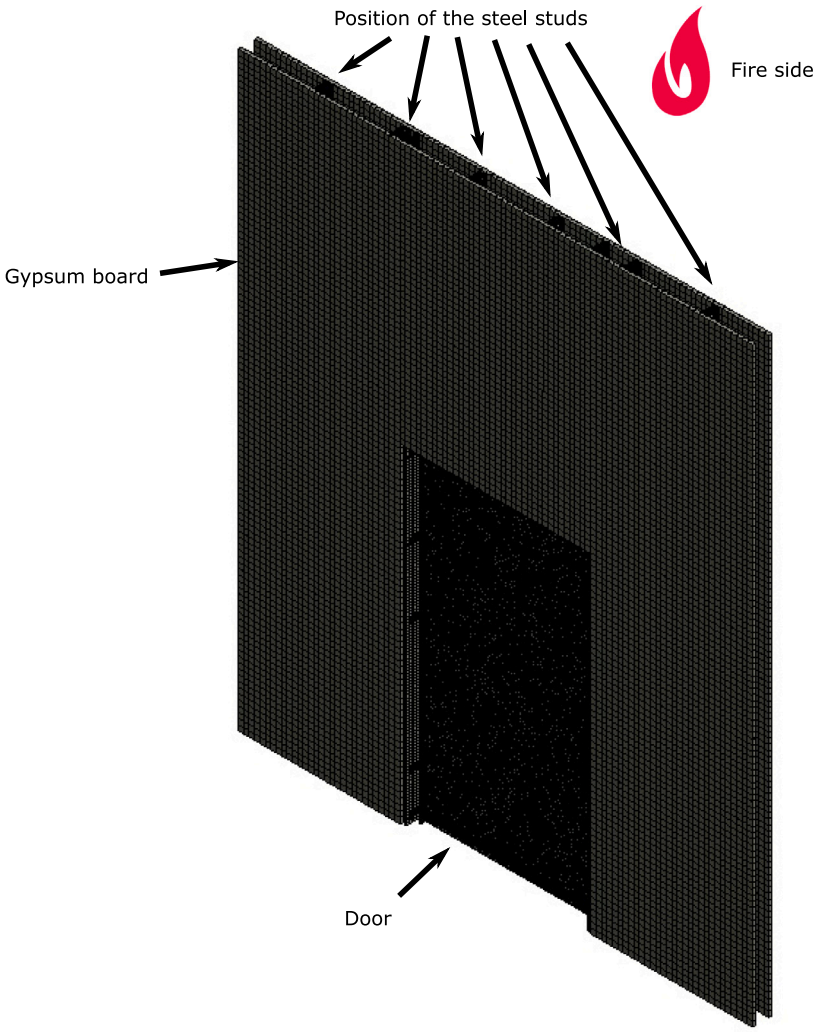

Fig. 13. Numerical grid for the structural analysis of the gypsum-sheathed stud wall for the case *DC*.

4.1.4. Radiative heat transfer in the porous structure

In the previous work of Prieler et al. [50] it was found that for thick gypsum blocks the consideration of the thermal radiative heat transfer within the porous structure is crucial for an accurate prediction. Although the entire wall does not consist of gypsum only, also mineral wool is a porous building material. Therefore, the radiative heat transfer was taken into account in the numerical model. For this purpose, the thermal conductivity of the fluid phase was adapted. This method is based on the work of Loeb [56], who assumed that a pore within a complex porous geometry can be approximated by simple geometries, such as cylinders or spheres. This method was successfully applied in [50,57–59]. Although in Prieler et al. [50] a porosity-corrected discrete ordinates model was slightly more accurate to predict the radiative heat transfer within porous structures, the calculation time would increase significantly. The radiative heat flux within a spherical pore can be calculated by Eq. (12), where the emissivity of the pore's surface is denoted as γ and σ is the Stefan–Boltzmann constant. Furthermore, the dimension of the pore and the temperature difference across the pore are represented by Δx and Δt. Based on Eq. (12) a so-called *radiant conductivity* can be derived (see Eq. (13)). In Eq. (13) the variable d stands for the pore diameter.

$$\dot{q}_{rad} = \frac{8}{3}\gamma\sigma T^3 \Delta t = \lambda_{rad}\frac{\Delta t}{\Delta x} \tag{12}$$

$$\lambda_{rad} = \frac{8}{3} d\gamma\sigma T^3 \tag{13}$$

Subsequently, the radiant conductivity can be added to the thermal conductivity of the fluid phase (e.g. the q-th phase) as given in Eq. (14). This means that no additional transport equation has to be solved to take the radiative heat transfer into account.

$$\lambda = \epsilon(\lambda_q + \lambda_{rad}) + (1-\epsilon)\lambda_{solid} \tag{14}$$

In the present study the emissivity of the pore's surface was set to a value of 1 and the pore diameters were chosen with values of 0.08 mm (gypsum) and 0.360 mm (mineral wool).

4.2. Structural analysis of the wall and the steel door

In this section the numerical methodology for the structural analysis of the wall and the door will be described. A presentation of the numerical grid as well as the boundary conditions (temperature profile) is given in Section 4.2.1. For modelling the gap formation between the door and the wall a contact formulation between the solid parts has to be done, which will be shown in Section 4.2.2. Other numerical settings and shortcomings of the presented methodology will be discussed in Sections 4.2.2 and 4.2.3.

4.2.1. Numerical grid

The numerical grid for the structural analysis is shown in Fig. 13, which consists of approx. 150,000 elements. The gypsum boards were modelled by hexahedrons and the steel shell of the door was made of

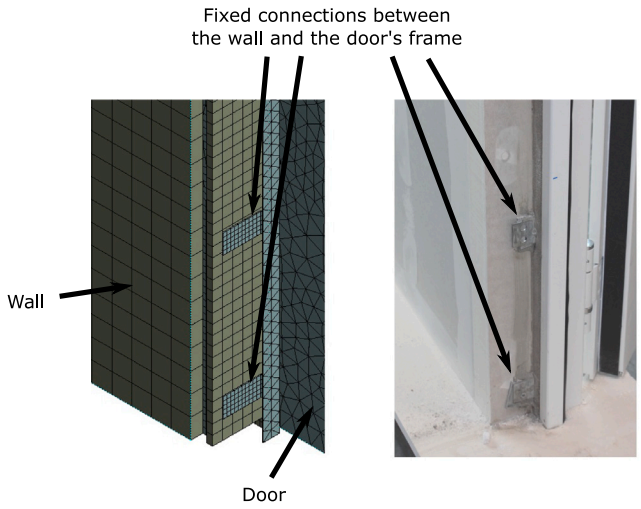

Fig. 14. Fixed connections between the wall and the door's frame.

tetrahedrons. In contrast to the solid 3-dimensional elements for the gypsum and the door, for the steel profiles in the wall shell elements (2-dimensional) were used. Similar numerical grids were created for the cases *DL* and *DR*. In Fig. 14 a more detailed view on the numerical grid at the fixed connections between the wall and the door's frame is presented. It can be seen that also for the solid connections hexahedrons were used.

4.2.2. Contact treatment between the solids

Since all components of the gypsum-sheathed stud walls as well as the door and the door's frame are in mechanical interaction, the contact faces has to be treated to allow or avoid relative (frictional) movement in accordance to the real experimental setting. Considering the gypsum-sheathed stud wall, the contact faces between the studs and the boards were treated as fixed contact over the entire length, although the connection between the boards and the steel studs is limited to certain fixing points in the real setting. Also the contact between the gypsum boards was a fixed connection. Further, fixed connections were applied between the wall and the door's frame as well as between the door and the frame at the position of the hinges, bolts and the door lock (see Fig. 7). For the fixed connections, the contact surfaces were defined by a bonded contact using the *multi-point constraint* (MPC) formulation (see [60]). Besides the fixed connections between the door and the frame, there are also contact faces, where a relative (frictional) movement is possible. Additionally, due to the thermal expansion/deformation process these contact faces can also separate from each other. Considering this effect is crucial for the prediction of the gap formation between the door and the wall/frame. The frictional contacts between the door and the frame were treated by the *augmented Lagrange method* proposed by Simo and Laursen [61]. This approach is a penalty-based method, where the normal and perpendicular contact forces are introduced. They can be seen as an additional virtual work (*penalty*) due to the violation of the contact condition (penetration between the bodies). Subsequently, small penetration between the surfaces is allowed in this approach, but was kept at a low level due to increasing the contact stiffness in the numerical model (value of 0.1). With an increasing contact stiffness the penetration between solid bodies would be lower. In the present work the maximum penetration between the door and the frame/wall was approx. 0.01 mm, which was found to be sufficient.

4.2.3. Boundary conditions and other numerical settings

Within the door, the gypsum board releases water vapour during the heating process, causing a pressure increase inside the steel shell. This effect was already examined in a work of Prieler et al. [62]. Thus, a linear pressure increase from ambient pressure to an over-pressure of 300 Pa was defined within the first 20 min testing time. From 20 to 30 min the pressure was constant at a level of 300 Pa. For the structural analysis the temperature trend in the wall (gypsum boards and steel studs) were used based on the thermal analysis of the wall. Since the numerical grid for the thermal analysis is different from the structural one, polynomial functions depending on the time and the local position in the wall were derived for the gypsum boards and the steel studs. This was done, because the heat transfer in the wall can be seen as 1-dimensional. In contrast to the wall, the heat transfer through the door and the door's frame is only 1-dimensional in the centre of the door. At the corners and edges, the assumption of a 1-dimensional heat transfer fails due to the thermal bridge over the steel shell. Subsequently, the heat transfer in the door and the frame was treated as 3-dimensional. Therefore, the calculated temperatures from the thermal analysis were stored for each time step and position in the door/frame in data files. The temperatures from these data files were mapped on the numerical grid for the structural analysis using a *profile preserved* mapping procedure, which was described in Prieler et al. [28].

The steel studs were defined with a fixed support at their lower edges (bottom of the wall), since they are fixed at the bottom in the real setting. At the upper edge the steel studs were placed in groves, which do not allow a movement perpendicular to the wall's surface. However, a small movement in the other directions is possible. At the left and right hand side of the wall, a fixed support for the gypsum boards was applied. For the structural analysis an auto-time stepping procedure was used, starting with an initial time step of 1/60 min. The algorithm automatically adapted the time step size depending on the convergence behaviour with a minimum and maximum time step size of 0.01/60 min and 5/60 min, respectively.

4.3. Shortcomings of the presented modelling approach

Due to the complexity of the overall heat transfer (heat conduction, water vapour transport etc.) in the wall and the test specimen as well as the mechanical interactions and deformation of the solid parts, some simplifications on the numerical model have to be done:

- The water vapour transport, condensation/evaporation and radiative heat transfer was only considered within the porous structures of the gypsum-sheathed stud wall. These effects were neglected within the porous structure inside the steel door. The reason for that is caused by the increasing pressure inside the steel shell of the door when water vapour is released from gypsum. This pressure increase led to numerical instabilities and no solution could be accomplished.
- During the fire resistance test, some of the gypsum boards were damaged or even fall off the wall at the fire exposed side. In the numerical model no failure of the gypsum boards was implemented. The damage of the gypsum boards at the fire exposed side would certainly effect the temperature inside the wall and its deformation (e.g. steel studs).
- Although the gap formation between the door and the wall was predicted in the present study, no direct calculation of the flue gas exit from the furnace, as presented for example in [29,30], was possible caused by the neglected simulation of the combustion process in the furnace. Nevertheless, with the proposed numerical model, this would also be possible as shown in Prieler et al. [30].
- The contact between the steel studs and the gypsum boards was defined as bonded contact over the entire height, which is not the case in the real setting. In the experimental setup the boards were fixed at certain positions at the steel studs.
- The intumescent material between the door and the frame was neglected in the numerical model.

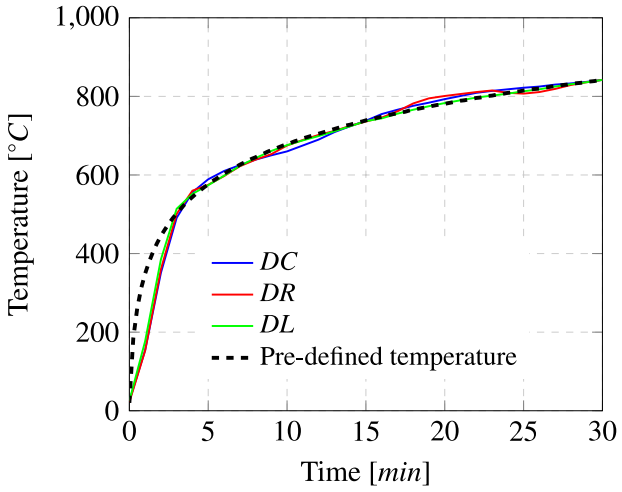

Fig. 15. Measured average temperature in the furnace during the FRT and pre-defined temperature according to [12].

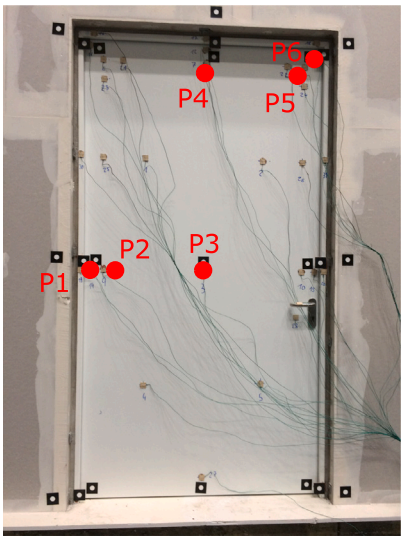

Fig. 16. Temperature measurement positions at the fire unexposed side of the door.

5. Results

In this section the experimental and numerical results will be compared to verify the applicability of the numerical approach to carry out the thermal and structural analysis of the test specimen and the gypsum-sheathed stud wall as well as their interactions (gap formation). As a consequence, the next sections will discuss the gas temperature in the furnace and the temperature of the test specimen (see Section 5.1). Section 5.2 will deal with the thermal analysis of the stud wall. Unfortunately, no temperature measurements were done within the wall during the FRT, thus the validation of the thermal model was done by comparison with data from literature (see Section 5.2.1). In Section 5.2.2 the validated thermal model was used for the gypsum-sheathed stud wall in the present study. The deformation process of the test specimen and the wall will be analysed in Sections 5.3 and 5.4. The gap formation and possible flue gas leakage will be shown in Section 5.5.

5.1. Gas phase combustion and temperature of the test specimen

As mentioned above, the gas phase combustion was not considered in the present study, however, the temperature in the furnace is a crucial boundary condition for the thermal analysis of the wall and the door. Furthermore, during the FRTs the average furnace temperature has to be in close accordance to the pre-defined temperature from [12], which is shown in Fig. 15. Furthermore, the average temperature for the three FRTs (*DC*, *DR*, *DL*) are presented in Fig. 15. The average temperature was determined based on the 12 plate thermocouples inside the furnace (see Section 3.1). It can be seen that the measured temperature in the furnace is in good agreement to the pre-defined temperature for all cases. There is only a deviation between the measurement and the pre-defined temperature at the beginning of the FRTs. This is caused by the thermal inertia of the plate thermocouples. For the thermal analysis the measured average temperatures were used for the boundary conditions at the fire exposed side of the wall and door.

At the door's fire unexposed side and its frame 31 thermocouples were placed to determine the thermal resistance of the door to the pre-defined temperature in the furnace. However, for the comparison with the numerical model 6 thermocouples were chosen as it can be seen in Fig. 16. The thermocouples at *P1* and *P6* were fixed 25 mm from the edge/corner of the door. Furthermore, three thermocouples were considered 100 mm from the edge/corner (*P2*, *P4* and *P5*). A comparison between the measurement and the thermal analysis will be also done at the centre of the door at *P3*. These 6 thermocouples should represent the overall temperature at the fire unexposed.

Since the thermal analysis of the solids was done with the temperature trend in the furnace as boundary condition, the thermal analysis for the door and the temperatures in the wall are the same for all three cases (*DC*, *DR*, *DL*). In Fig. 17 the calculated temperatures were compared to the measured data for the case *DC*. The highest temperature was observed in the experiment and simulation 25 mm (*P1* and *P6*) from the corner/edge. This is caused by the lower thermal resistance of the steel shell of the door compared to the mineral wool and gypsum board at the centre of the door. It can be seen in Fig. 17 that the simulation over-predicted the temperature at the door's corner/edge. Until the end of the experiment the calculated temperature was 24 °C and 50 °C higher at *P1* and *P6* (also compare Fig. 18), respectively. When moving from the door's corner/edge to the centre (*P3*) the simulation clearly showed a lower temperature compared to the measurement. As already mentioned, the thermal analysis of the test specimen neglected the effect of water vapour and condensation/evaporation inside the steel shell. Since water vapour is transported in the porous structure of gypsum and mineral wool, the water vapour gets in contact with the steel at the fire unexposed side of the door. At the beginning of the FRT the steel temperature is lower than 100 °C and the water vapour condenses there, releasing the latent heat, which is leading to an improved heat transfer at the fire unexposed side. Therefore, the steel is heated up much faster to temperatures between 90 and 100 °C.

It can be concluded that due to the missing modelling of the water vapour inside the door, the temperature at the door's centre is too low. However, in the vicinity of the corners and edges the temperature fits much better with the experimental data. Furthermore, at all measurement positions near the door's corner/edges the temperature started to rise earlier compared to the measurement. This effect is caused by the simplified boundary condition at the fire exposed side, where the convective and radiative heat transfer was defined. In contrast, the fluid flow and heat transfer at the fire exposed side during the FRT is more complex. Overall, the temperatures can be used for the structural analysis.

In Fig. 18 the simulated and measured temperatures at the end of the FRTs (30 min) for each case are presented (*DC*, *DR*, *DL*). It can be seen that in all experiments the door temperature was very similar, with the highest temperatures of approx. 200 °C 25 mm from the corner and edge. The temperature at the other positions was between 80 and 103 °C. Overall, the numerical results showed a good agreement with the experiments, except the centre of the door, where the temperature

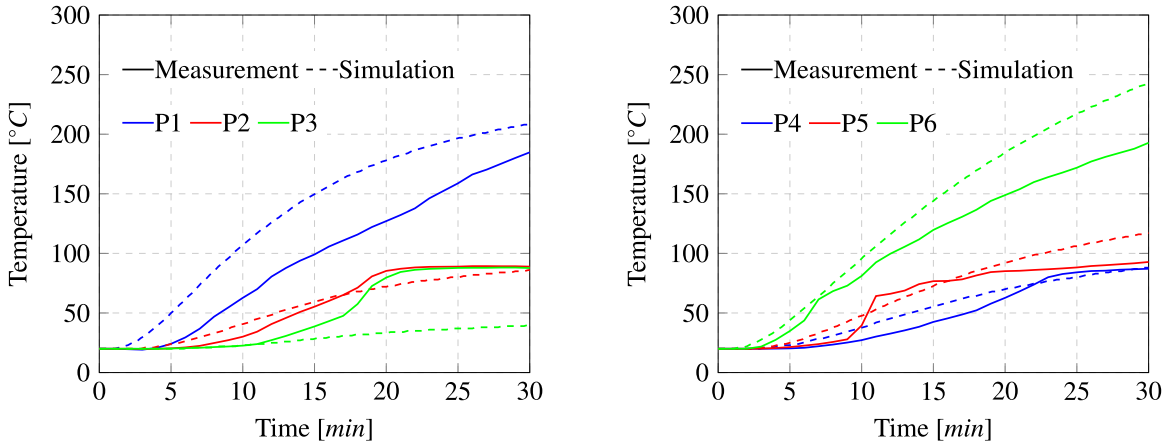

Fig. 17. Measured and simulated temperatures at the door's fire unexposed side for the case *DC*.

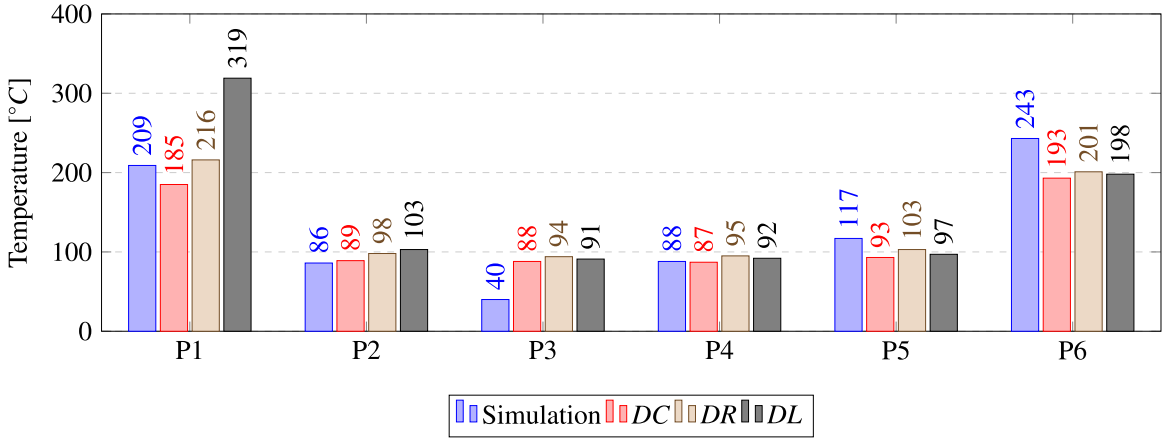

Fig. 18. Measured and simulated temperatures at the door's fire unexposed side after 30 min testing time.

was clearly under-predicted. Furthermore, at *P1* after 30 min in the experiment *DL* the temperature is significantly higher compared to the other FRTs and the simulation (see Fig. 18). In that case the flue gases from the furnace were leaked to the ambient side through a gap between the door and the wall near this thermocouple, which was caused by the deformation process. So, the thermocouple was heated up due to the direct contact with the hot flue gases.

5.2. Temperatures in the stud wall

In this section the thermal model for the wall, including the water vapour transport, condensation/evaporation and radiative heat transfer will be validated using data from literature (see Section 5.2.1). After the validation process the numerical model will be applied to predict the heat transfer in the gypsum-sheathed stud wall, which was used in the FRTs in the present study (see Section 5.2.2).

5.2.1. Validation of the heat transfer model for the gypsum-sheathed stud wall

The numerical results of the heat transfer model used for the gypsum-sheathed stud wall will be compared to the experimental data from Nassif et al. [40]. Nassif et al. investigated a stud wall exposed to standard fire conditions where the steel studs were covered by two gypsum boards on each side, which is the same construction used in the present study. The only difference is the thickness of the wall. The thickness of the mineral wool between the gypsum boards was 75 mm in the study of Nassif et al. in contrast to 100 mm in the present study. Thus, the model in Fig. 12 was adapted for the validation process to represent the wall investigated by Nassif et al.

In Fig. 19 the experimental data from Nassif et al. (solid lines) and the numerical results (dashed lines) are presented at the measurement positions *T1*, *T2* and *T3*, which are placed in accordance to Fig. 12. It can be seen that at each position there is a phase of rapid heating up to approx. 100 °C, which is caused by the condensation of water vapour from the gypsum. This heating process is slightly over-predicted by the numerical model and means that the water vapour transport inside the porous structure is faster in the simulation and the water condenses earlier at these positions. From Fig. 12 a period of nearly constant temperature at approx. 100 °C can be observed. During this period the condensed water absorbs the heat from the fire side and will be re-evaporated. Based on the length of the temperature plateau, the numerical model can predict the re-evaporation of the condensed water with high accuracy. After the water was re-evaporated the temperature increase is faster and a close accordance between the numerical model and the experimental data can be found.

In Fig. 20 the temperature data from Nassif et al. (solid lines) and the numerical model are shown at the measurement positions *T4* and *T5*. As mentioned above, the numerical model slightly over-predicted the water vapour transport. Due to this fact, the heating inside the wall starts earlier in the simulation. However, this effect is very sensitive on the pressure inside the furnace. In the experiments the pressure in the furnace was observed and an over-pressure of 10 Pa was chosen in the numerical simulation (see Section 4.1.1), which is presented in Fig. 20 by the dashed lines. To highlight the sensitivity of the heating process on the pressure inside the furnace, an additional simulation

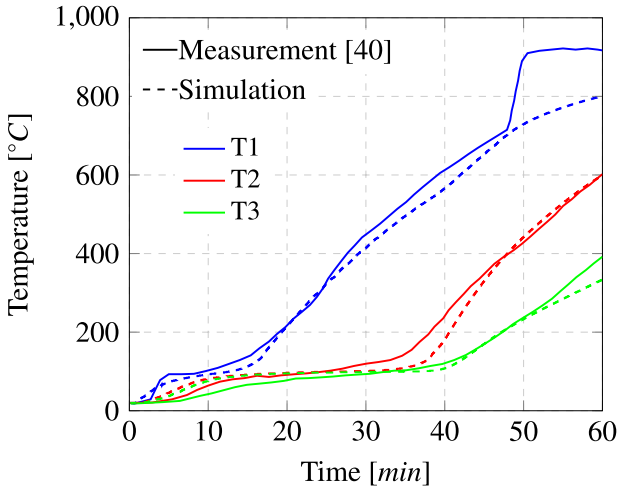

Fig. 19. Measured temperatures according to [40] and calculated temperatures at *T1*, *T2* and *T3* within the gypsum-sheathed stud wall.

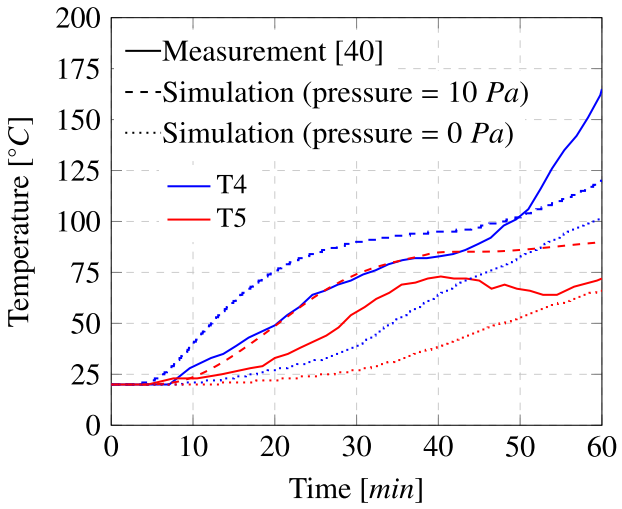

Fig. 20. Measured temperatures according to [40] and calculated temperatures at *T4* and *T5* within the gypsum-sheathed stud wall.

was carried out without over-pressure (dotted lines). It was found that without over-pressure the heating process is delayed. Unfortunately, Nassif et al. did not mention the pressure inside the furnace in [40]. In contrast, the pressure was observed in the present study and will be used as boundary condition in the simulation in Section 5.2.2.

The numerical results in this section showed a good agreement to the measured data and the numerical model is capable to predict the heating process caused by the water condensation, etc.

5.2.2. Temperatures in the gypsum-sheathed stud wall used in the present study

In Fig. 21 the calculated temperatures within the gypsum-sheathed stud wall, which was used in the present study, are presented during the FRTs. Similar to the simulation in Section 5.2.1, at each position the heating starts when water vapour condenses followed by a phase of nearly constant temperature at approx. 100 °C. At *T1* the water was re-evaporated after approx. 15 min and an increase of the temperature can be observed. The measurement positions in direct contact with the steel stud (*T2* to *T4*) are heated up by the condensing water between 90 and 100 °C during the FRT. After 30 min the re-evaporation was not finished, and, thus, the temperature of the steel stud was not increasing above 100 °C. In Fig. 22 (left) the volume fraction of condensed water

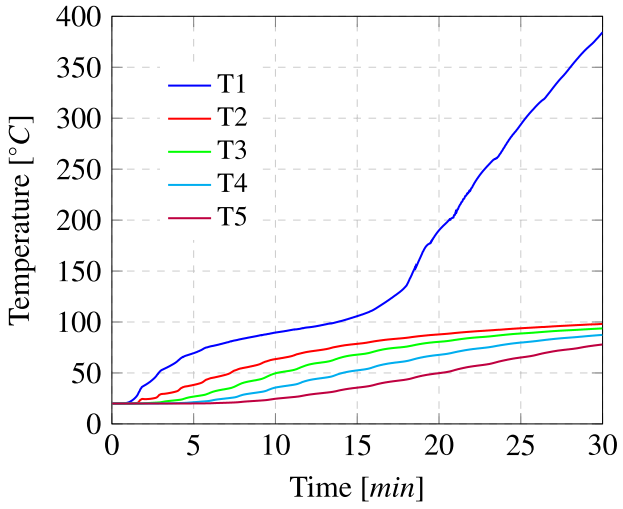

Fig. 21. Calculated temperatures within the gypsum-sheathed stud wall used in the present study.

in the fluid within the porous gypsum is shown. From the figure it can be seen that at the measurement positions around the steel stud condensed water is still present after the FRT. Thus, the temperature of the steel stud is limited to a maximum temperature of approx. 100 °C (see Fig. 22 (right)). In addition to the temperatures in the steel door from Section 5.1, the temperatures within the stud wall were used for the structural analysis.

5.3. Deformation of the steel door

For the measurement of the door's deformation 9 observation points were arranged at the door's fire unexposed side (see red dots in Fig. 23). In addition, 7 measurement points were fixed at the wall marked by the blue dots in Fig. 23. The placement of the measurement positions was the same in all three FRTs. It has to be mentioned that negative values for the deformation represent a deformation to the fire exposed side and positive values stand for a displacement to the ambient side.

In Fig. 24 the deformation of the door for the case *DC* is shown at the door's upper edge (*D_A*, *D_B*, *D_C*) and its half height (*D_D*, *D_E*, *D_F*). At the door's upper edge (see Fig. 24 (left)) the measured deformation is shown by the solid lines. It can be seen that the door's deformation is high at the beginning of the experiment (10 min). After 10 min the deformation is quite constant with a level of approx. −30 mm at *D_B* and −18 mm at *D_A* and *D_C* until the end of the experiment. The simulation predicted a similar trend for the central position *D_B*, whereas the calculated deformation is lower at the beginning but steadily increasing until the end of the experiment. At the end of the experiment the simulation results showed a good agreement to the measured data. Furthermore, at the centre of the door *D_E* the simulation predicted a deformation with good agreement to the experiment (see Fig. 24 (right)). However, the simulation underpredicted the deformation at the door's edge (*D_D* and *D_F*), where a deformation of −50 to −45 mm was detected. The reason for that can be found in Fig. 25. Here, the failure of the bolt (left side of the door) and the door's lock (right side of the door) can be seen. During the experiment these parts failed to safely connect the door leaf with its frame. Therefore, the assumption of a fixed contact at these positions in the simulation is not valid anymore, leading to a much lower deformation.

Furthermore, the comparison between the measured and predicted deformation at the door's upper edge can be seen in Fig. 26 for the case *DL* and *DR*. At the corners (*D_A* and *D_C*) of the door the measured deformation is very similar to the case *DC* with a deformation of

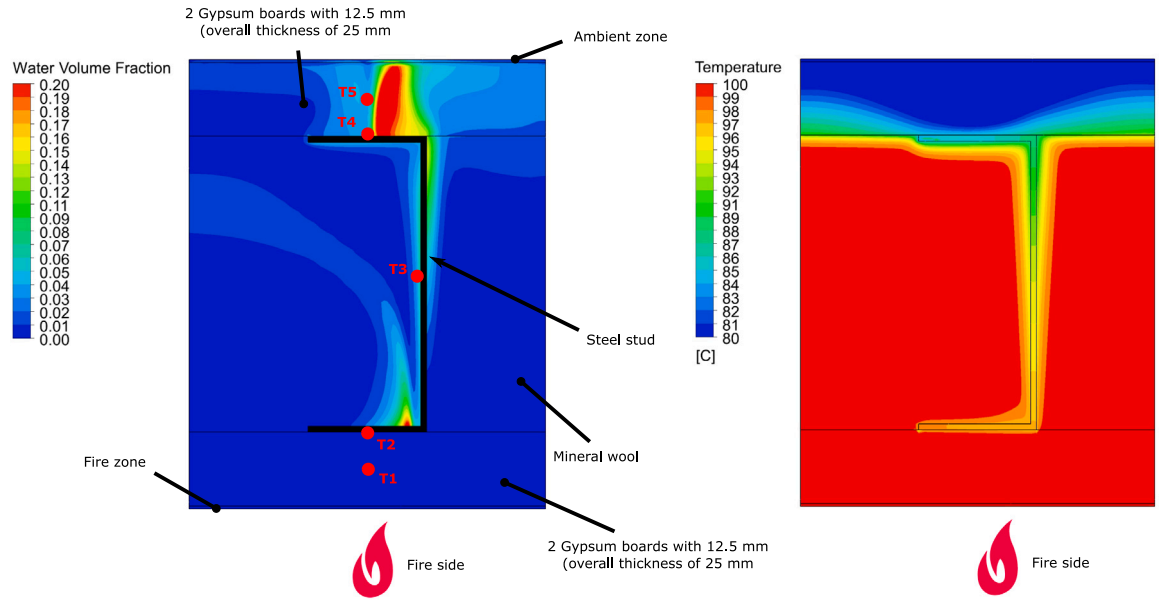

Fig. 22. Calculated volume fraction of condensed water (left) and temperature (right) in the gypsum-sheathed stud wall et the end of the FRT.

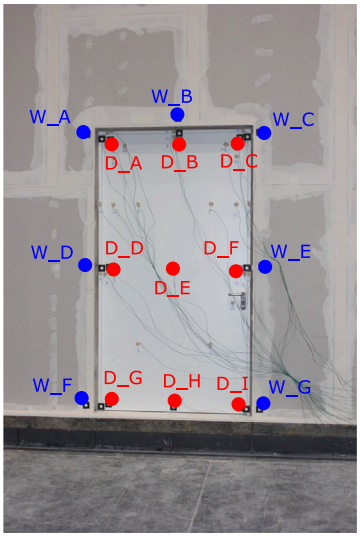

Fig. 23. Deformation measurement positions at the fire unexposed side of the door (red dots) and the wall (blue dots). (For interpretation of the references to colour in this figure legend, the reader is referred to the web version of this article.)

approx. −20 mm at the end of the FRTs. It has to be mentioned that the deformation to the fire exposed side is starting later when the door is in the right position *DR* compared to *DL*. In contrast to the case *DC*, the simulation predicted a deformation of approx. −12 mm at *D_A* and *D_C*, which is a little bit lower than the measured values. Considering the measurement position *D_B* in the middle, the simulation results showed a better agreement to the experiment. This is highlighted for the case *DC*, where the transient behaviour of the deformation as well as the deformation magnitude is in close accordance. For the case *DR* the transient trend is different, which can be also seen in the following figure and the deformation of the wall. This might be an effect of the early failure of the gypsum boards discussed in Section 5.4.

In Fig. 27 the deformation at the door's half height is presented for the cases *DL* and *DR*. As already seen in the case *DC*, the deformation in the middle of the door (*D_E*) can be predicted by the numerical approach and similar results were observed the FRTs. But at the edges of the door (*D_D* and *D_E*) the same effect as shown in Fig. 25 was detected during the FRT, which leads to a high deformation there (between −50 and −40 mm). In the FRT of case *DL* the observation point at *D_D* was damaged after 22 min. Since the contact between the door's frame/wall and the door is defined as fixed during the entire simulation of the FRT, the predicted deformation at the edges is under-predicted with values around −15 to −10 mm.

At the bottom of the door (*D_G*, *D_H* and *D_I*) a very low deformation was observed, thus this is not presented in a separate chart here. Only at the middle position (*D_H*) the door was deformed about −8 mm in all FRTs, whereas the other measurement positions slightly deformed to the fire unexposed side.

From the results it can be concluded that the numerical model is capable to predict the deformation of the door, since the deformation in the middle of the door (upper edge and door's half height) is in good agreement to the measurement. However, the contact treatment between the wall and the door seems to be a potential risk for the accuracy of the simulation at the door's edges and corners. This was found by the failure of bolts and the door lock and its effect on the measured data. It has to be mentioned that for the case *DR* the predicted trend of the deformation is different from the measured deformation. Especially the time period at the beginning of the FRT (5 min), where no deformation occurred in the experiment, was not covered by the simulation. Thus, for the case *DR* the numerical model has to be improved for the better prediction (e.g. failure modes for the gypsum boards, bolts and door lock).

5.4. Deformation of the gypsum-sheathed stud wall

Considering the case *DC*, Fig. 28 (left) shows the measured and simulated deformation of the wall at the upper edge of the door and the door's half height as well as the bottom (Fig. 28 (right)). It can be seen that at the door's upper edge the measured deformation of the wall is similar at all three positions. First, the deformation of the wall is increasing up to a value of approx. −15 mm in 10 min of the FRT. After that the deformation is quite constant until the end of the experiment with a value of about −19 mm. The simulation predicted a transient behaviour, which is very similar to the observations during the FRT. At all three positions the deformation is very similar. However, the magnitude of the deformation is much lower with approx. −9 mm after 30 min. The observed deformation during the FRT at the door's half height (*W_D*, *W_E*) is very similar to the results at the door's upper

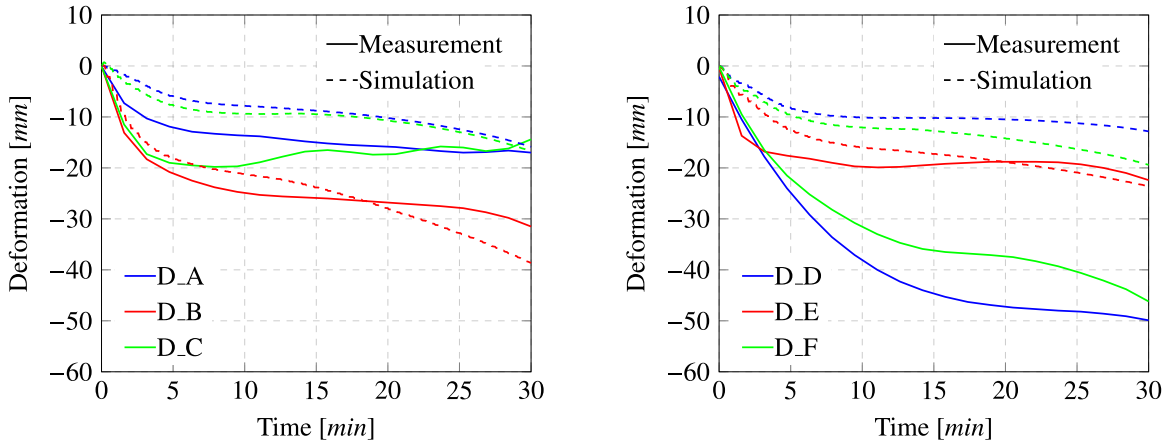

Fig. 24. Measured and calculated deformation of the door when the door is in the central position (*DC*).

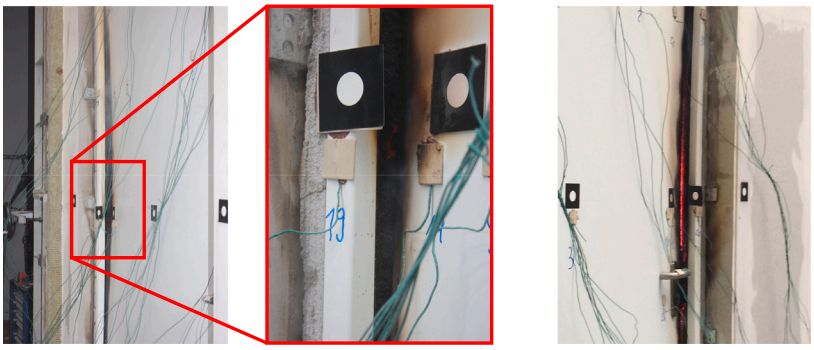

Fig. 25. Failure of the bolt connection between door and frame (left) and door lock (right) for the case *DC*.

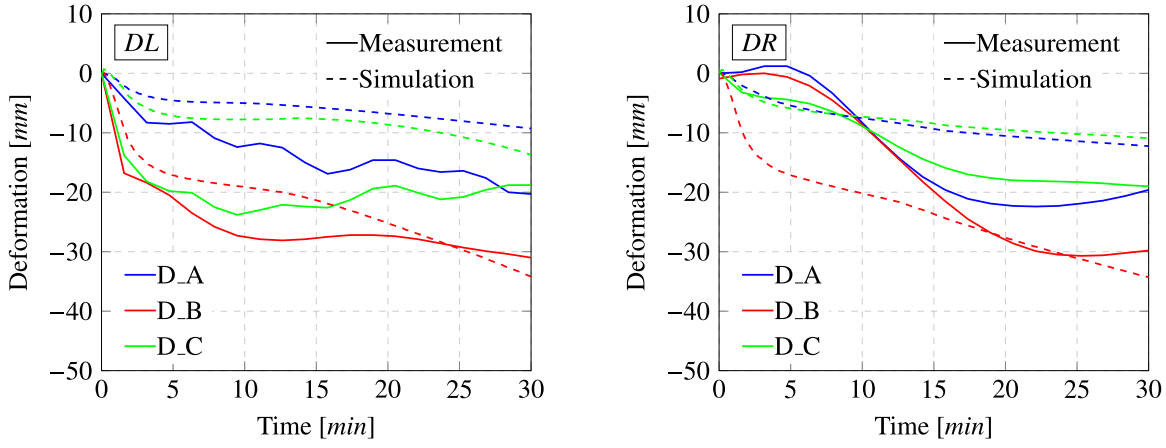

Fig. 26. Measured and calculated deformation of the door at *D_A*, *D_B* and *D_C* for the cases when the door is in the left position (*DL*) and the door is in the right position (*DR*).

edge, leading to a deformation of approx. −19 mm after 30 min. Here, the numerical simulation predicted a deformation which is slightly higher compared to the door's upper edge. The simulation predicted a deformation of approx. −15 mm after 30 min, which is in a better agreement to the experiment. The higher deformation at the door's half height calculated by the FEM simulation is caused by the fixed connections to the door. The forces on the wall due to the thermal expansion of the door are transported to the wall, which is not the case at the upper edge. At the bottom of the wall (*W_F*, *W_G*) hardly any deformation can be found in the experiment and simulation.

The cases *DL* and *DR* showed a similar deformation behaviour (transient and magnitude) as case *DC* at the door's upper edge (see Fig. 29). The measurement showed an increase of the deformation up to approx. −20 to −10 mm for the case *DL*, followed by a phase with quite constant deformation. Due to the asymmetric position of the door, the deformation on the left hand side of the door (*W_A*) is 8 mm lower compared to *W_C*. Considering the case *DC* in Fig. 28 the deformation was the same at all positions at the door's upper edge (*W_A*, *W_B*, *W_C*). The FEM simulation for the case *DL* also predicted a too low deformation. However, the asymmetric behaviour can be identified in the simulation. At position *W_B* and *W_C* the predicted deformation was approx. −5 mm compared to −2 mm at *W_A* at the end of the FRT. When considering the case *DR*, the asymmetric behaviour is vice versa compared to *DL*. This can be seen by the high deformation at *W_A* after 30 min with a value of −23 mm compared to −14 mm at *W_C*. The asymmetric behaviour for the case *DR* was also determined by the

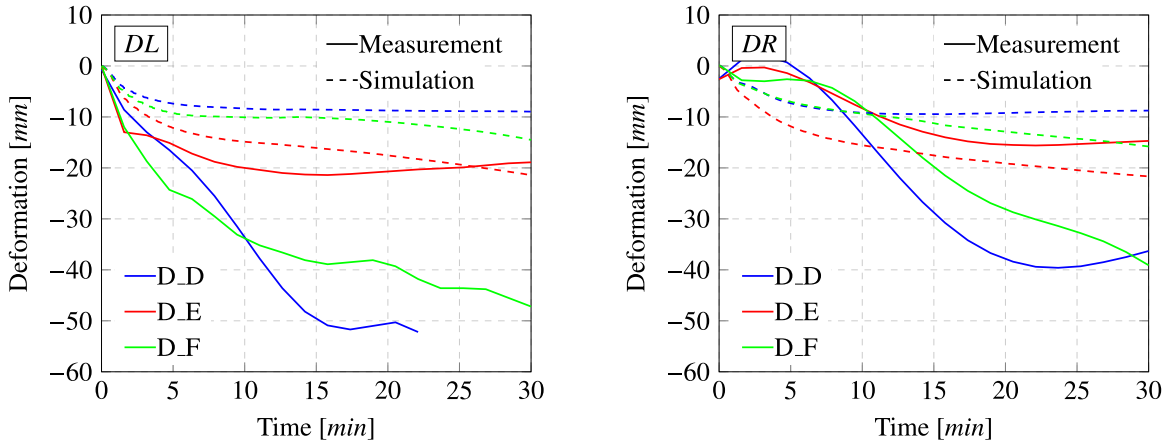

Fig. 27. Measured and calculated deformation of the door at *D_D*, *D_E* and *D_F* for the cases when the door is in the left position (*DL*) and the door is in the right position (*DR*).

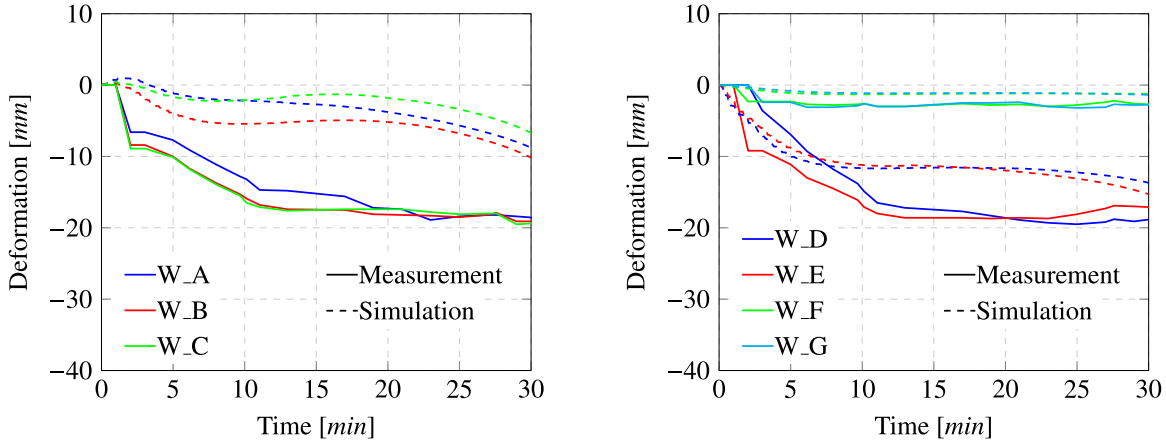

Fig. 28. Measured and calculated deformation of the wall when the door is in the central position (*DC*).

simulation, although the magnitude of the deformation is much lower. A reason for the higher measured deformation of the wall compared to the simulation for all three FRTs is caused by the failure of the gypsum boards at the fire exposed side. Considering the deformation of the case *DR* in Fig. 29, it can be seen that the deformation suddenly increases after approx. 10 min. This is caused by the failure of both gypsum boards at the same time. This is illustrated in Fig. 30 (left). Both gypsum boards fell off and the steel studs were directly exposed to the fire, leading to a higher temperature of the studs. This effect was not covered by the simulation, since a failure mode is missing. Furthermore, it can be seen that also the mineral wool in the wall was damaged exposing a gap to the gypsum boards at the fire unexposed side (see Fig. 30 (red circle)). In the other FRTs it was found that only one gypsum board was falling off the fire exposed side, whereas the second one still covered the steel studs (see 30 (right)). As a consequence, the lower wall deformation predicted by the simulation can be explained by two facts: (i) the steel studs in the FRTs have higher temperature due to the failure of gypsum boards and direct exposure to the fire and (ii) the total structural integrity of all gypsum boards in the simulation was assumed, although some boards were falling off and did not contribute to the mechanical stability of the wall anymore.

5.5. Gap modelling between wall and door

In addition to the deformation of the door and the wall, in this section the gap formation between the door and the wall will be discussed. In Fig. 31 (left) the overall deformation of the wall and the door is presented after 30 min. Since both parts (door and wall) were analysed simultaneously, the gap formation between the contact faces with a sliding formulation can be determined. On the left hand side of the door, hardly any gap formation was found in the simulation. This was also confirmed by the observations during the FRTs. Only when the bolt's connection to the door's frame got damaged (see Fig. 25) a gap formation was observed in the FRT. However, in the simulation the failure of fixed connections, such as bolts, was not considered. Also on the upper edge of the door the gap formation was very low in all FRTs. The most prominent gap formation occurred on the right hand side of the door (side of the door lock), which is shown in Fig. 31 (right). Right above the door lock, a gap formation was observed in all three FRTs. Due to the partial failure of the door lock during the FRT, the gap was not in the middle between the door lock and the upper edge of the door. So, the gap was more shifted downwards to the position of the lock. In contrast, the simulation showed that the highest gap formation of approx. 7 mm was in the middle between the lock and the upper edge of the door, caused by the missing failure of the lock in the simulation. Nevertheless, the simulation showed that the gap formation can be predicted by the numerical approach.

6. Conclusion and outlook

In the present paper FRTs of a fire safety steel door (test specimen) embedded in a gypsum-sheathed stud wall were carried out and a numerical methodology to predict the temperature, deformation and gap formation during the test was presented. The measured temperatures, deformation and gap formation were compared to the simulation results, which determined the applicability of the numerical approach. Based on the results the following conclusions can be made:

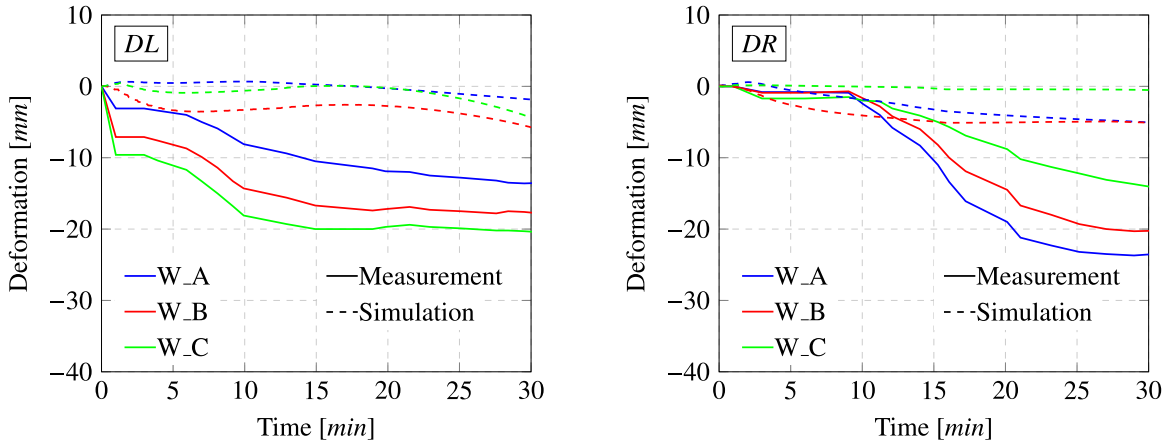

Fig. 29. Measured and calculated deformation of the wall at *W_A*, *W_B* and *W_C* for the cases when the door is in the left position (*DL*) and the door is in the right position (*DR*).

Fig. 30. Failure of gypsum plasterboards when the door is in right position (*DR*) and the door is in central position (*DC*). (For interpretation of the references to colour in this figure legend, the reader is referred to the web version of this article.)

- The simulation methodology for the overall heat transfer in the wall, including heat conduction, water vapour transport, condensation/evaporation and radiative heat transfer showed a good performance when compared to the validation data and was used to accurately predict the temperature within the gypsum-sheathed stud wall. However, the failure of the gypsum board was not considered in the numerical model, which means that the steel studs inside could reach higher temperatures in the experiment.
- The predicted temperatures at the steel door showed a reasonable agreement with the measured data although some simplifications in the numerical model had to be done. Only at the door's centre the calculated temperature was lower than the measured one. This was caused by the missing water vapour transport inside the steel shell of the door.
- When the measured and calculated deformation of the door was compared, it was found that the structural analysis was capable to predict the door's deformation in its centre accurately. However, in the vicinity of the bolts and the door lock the predicted deformation was under-estimated. This effect was explained my the failure of the bolts and door lock during the FRTs, leading to a higher deformation of the door when losing the mechanical interaction to the wall.
- The structural analysis of the wall showed a similar trend of the deformation compared to the measurement, although the magnitude of the deformation was too low in all cases. During the FRTs the failure of the gypsum boards was affecting the heating of the steel studs in the wall, which reached higher temperatures than calculated in the numerical model. Thus, the deformation of the steel studs and wall was higher.
- The position of the gap formation between the wall and the door was accurately identified by the simulation.

As a consequence, the proposed numerical methodology can be used for FRTs where a test specimen is embedded in a gypsum-sheathed stud wall to predict the temperature, deformation and gap formation. However, to increase the accuracy of the simulation the following points should be addressed in future investigations:

- Consideration of a failure model for the gypsum boards.
- Consideration of the failure/damage of fixed connections between the door and the wall (e.g. bolts, door lock).
- Modelling of the water vapour transport and condensation/evaporation inside the steel shell of the door.

CRediT authorship contribution statement

Rene Prieler: Conceptualization, Methodology, Investigation, Writing – original draft, Writing – review & editing, Visualization, Supervision, Funding acquisition. **Benjamin Ortner:** Investigation. **Thomas Pfeifer:** Investigation. **Peter Kitzmüller:** Investigation, Writing – review & editing. **Stefan Thumser:** Project administration, Funding acquisition. **Günther Schwabegger:** Project administration, Funding acquisition. **Christoph Hochenauer:** Writing – review & editing, Supervision, Project administration, Funding acquisition.

Declaration of competing interest

The authors declare the following financial interests/personal relationships which may be considered as potential competing interests: Rene Prieler reports financial support was provided by Austrian Research Promotion Agency.

Data availability

Data will be made available on request.

Acknowledgements

This work was financially supported by the Austrian Research Promotion Agency (FFG), "Virtuelle Bauteilprüfung mittels gekoppelter CFD/FEM-Brandsimulation" (project 857075, eCall 6846234) and "Entwicklung von CFD/FEM Brandsimulationsmodellen mit Fokus auf Holz- und Gipsbauteile sowie komplexen Konstruktionen" (project 876469, eCall 28585806).

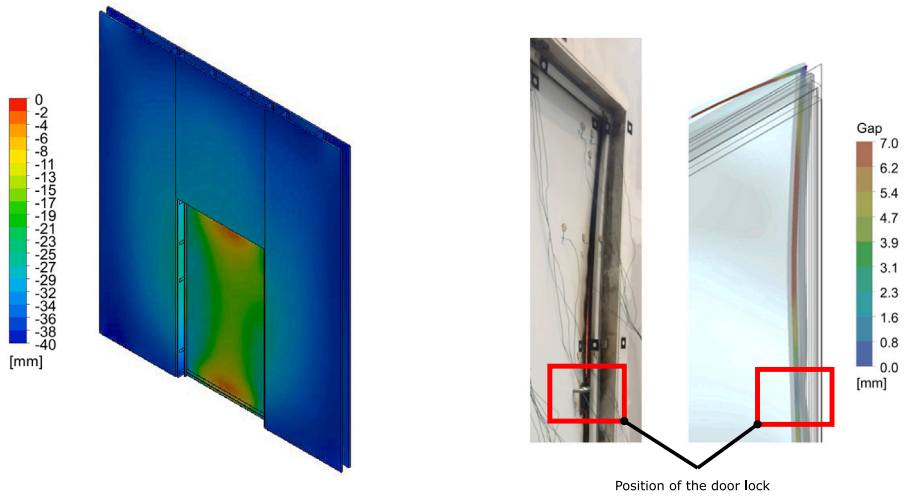

Fig. 31. Calculated deformation of the wall and the door after 30 min (left) and gap formation above the door lock (right) for the case *DC*.

References

[1] R. Gann, A. Hamins, K. McGrattan, H. Nelson, T. Ohlemiller, K. Prasad, W. Pitts, Reconstruction of the fires and thermal environment in world trade center buildings 1, 2, and 7, Fire Technol. 49 (2013) 679–707, http://dx.doi.org/10.1007/s10694-012-0288-3.

[2] I. Fletcher, A. Borg, N. Hitchen, S. Welch, in: Edinburgh Research Archive (Ed.), Performance of Concrete in Fire: a Review of the State of the Art, with a Case Study of the Windsor Tower Fire, 2006, URL https://era.ed.ac.uk/handle/1842/1987.

[3] X. Dai, S. Welch, A. Usmani, A critical review of "travelling fire" scenarios for performance-based structural engineering, Fire Saf. J. 91 (2017) 568–578, http://dx.doi.org/10.1016/j.firesaf.2017.04.001.

[4] N. Alam, A. Nadjai, M. Charlier, O. Vassart, S. Welch, J. Sjöström, X. Dai, Large scale travelling fire tests with open ventilation conditions and their effect on the surrounding steel structure– The second fire test, J. Constr. Steel Res. 188 (2022) 107032, http://dx.doi.org/10.1016/j.jcsr.2021.107032.

[5] A. Nadjai, A. Naveed, M. Charlier, O. Vassart, S. Welch, A. Glorieux, J. Sjostrom, Large scale fire test: The development of a travelling fire in open ventilation conditions and its influence on the surrounding steel structure, Fire Saf. J. 130 (2022) 103575, http://dx.doi.org/10.1016/j.firesaf.2022.103575.

[6] L. Li, B. Liu, W. Zheng, X. Wu, L. Song, W. Dong, Investigation and numerical reconstruction of a full-scale electric bicycle fire experiment in high-rise residential building, Case Stud. Therm. Eng. 37 (2022) 102304, http://dx.doi.org/10.1016/j.csite.2022.102304.

[7] Z. Nan, X. Dai, H. Chen, S. Welch, A. Usmani, A numerical investigation of 3D structural behaviour for steel-composite structures under various travelling fire scenarios, Eng. Struct. 267 (2022) 114587, http://dx.doi.org/10.1016/j.engstruct.2022.114587.

[8] J. Martinez, A. Jeffers, Structural response of steel-concrete composite floor systems under traveling fires, J. Constr. Steel Res. 186 (2021) 106926, http://dx.doi.org/10.1016/j.jcsr.2021.106926.

[9] S. Shan, W. Pan, Collapse mechanisms of multi-story steel-framed modular structures under fire scenarios, J. Constr. Steel Res. 196 (2022) 107419, http://dx.doi.org/10.1016/j.jcsr.2022.107419.

[10] J. Downer, When the chick hits the fan: Representativeness and reproducibility in technological tests, Soc. Stud. Sci. 37 (1) (2007) 7–26, http://dx.doi.org/10.1177/0306312706064235.

[11] J. Gales, C. Maluk, L. Bisby, Large-scale structural fire testing - how did we get here, where are we, and where are we going? in: 15th International Conference on Experimental Mechanics, Porto, Portugal, 2012.

[12] European Committe for Standardization CEN, European Standard EN 1363–1: Fire Resistance Test-Part 1: General Requirements, Brussels, Belgium, 2012.

[13] S. Welch, S. Miles, S. Kumar, T. Lemaire, A. Chan, FIRESTRUC - Integrating advanced three-dimensional modelling methodologies for predicting thermo-mechanical behaviour of steel and composite structures subjected to natural fires, Fire Saf. Sci. 9 (2009) 1315–1326, http://dx.doi.org/10.3801/IAFSS.FSS.9-1315.

[14] N. Tondini, O. Vassart, J.-M. Franssen, Development of an interface between CFD and FE software, in: 7th International Conference on Structures in Fire, Zurich, Switzerland, 2012.

[15] S. Welch, P. Rubini, Three dimensional simulation of a fire resistance furnace, in: 5th International Symposium on Fire Safety Science, Melbourne, Australia, 1997, pp. 1009–1020.

[16] K. Ghazi Wakili, L. Wullschleger, E. Hugi, Thermal behaviour of a steel door frame subjected to the standard fire of ISO 834: Measurements, numerical simulation and parameter study, Fire Saf. J. 43 (2008) 325–333, http://dx.doi.org/10.1016/j.firesaf.2007.11.003.

[17] E. Hugi, K. Ghazi Wakili, L. Wullschleger, Measured and calculated temperature evolution on the room side of a butted steel door frame subjected to the standard fire of ISO 834, Fire Saf. J. 44 (2009) 808–812, http://dx.doi.org/10.1016/j.firesaf.2009.02.003.

[18] K. Prasad, H.R. Baum, Coupled fire dynamics and thermal response of complex building structures, Proc. Combust. Inst. 30 (2005) 2255–2262, http://dx.doi.org/10.1016/j.proci.2004.08.118.

[19] X. Yu, A.E. Jeffers, A comparison of subcycling algorithms for bridging disparities in temporal scale between the fire and solid domains, Fire Saf. J. 59 (2013) 55–61, http://dx.doi.org/10.1016/j.firesaf.2013.03.011.

[20] D.I. Kolaitis, M.A. Founti, Development of a solid reaction kinetics gypsum dehydration model appropriate for CFD simulation of gypsum plasterboard wall assemblies exposed to fire, Fire Saf. J. 58 (2013) 151–159, http://dx.doi.org/10.1016/j.firesaf.2013.01.029.

[21] D.I. Kolaitis, E.K. Asimakopoulou, M.A. Founti, Fire behaviour of gypsum plasterboard wall assemblies: CFD simulation of a full-scale residential building, Case Stud. Fire Saf. 7 (2017) 23–35, http://dx.doi.org/10.1016/j.csfs.2016.11.001.

[22] R. Prieler, M. Mayrhofer, M. Eichhorn-Gruber, G. Schwabegger, C. Hochenauer, A numerical methodology to predict the gas/solid interaction in fire resistance tests, in: 10th Interantional Conference on Structures in Fire, Belfast, UK, 2018, pp. 383–390.

[23] R. Prieler, M. Mayrhofer, M. Eichhorn-Gruber, G. Schwabegger, C. Hochenauer, Development of a numerical approach based on coupled CFD/FEM analysis for virtual fire resistance tests—Part a: Thermal analysis of the gas phase combustion and different test specimens, Fire Mater. 43 (2018) 34–50, http://dx.doi.org/10.1002/fam.2666.

[24] J. Alos-Moya, I. Paya-Zaforteza, M. Garlock, E. Loma-Ossorio, D. Schiffner, A. Hospitaler, Analysis of a bridge failure due to fire using computational fluid dynamics and finite element models, Eng. Struct. 68 (2014) 96–110, http://dx.doi.org/10.1016/j.engstruct.2014.02.022.

[25] C. Zhang, J. Silva, C. Weinschenk, D. Kamikawa, Y. Hasemi, Simulation methodology for coupled fire-structure analysis: Modeling localized fire tests on a steel column, Fire Technol. 52 (2016) 239–262, http://dx.doi.org/10.1007/s10694-015-0495-9.

[26] M. Malendowski, A. Glema, Development and implementation of coupling method for CFD-FEM analyses of steel structures in natural fire, Procedia Eng. 172 (2017) 692–700, http://dx.doi.org/10.1016/j.proeng.2017.02.082.

[27] M.A. Orabi, A.A. Khan, L. Jiang, T. Yarlagadda, J. Torero, A. Usmani, Integrated nonlinear structural simulation of composite buildings in fire, Eng. Struct. 252 (2022) 113593, http://dx.doi.org/10.1016/j.engstruct.2021.113593.

[28] R. Prieler, H. Gerhardter, M. Landfahrer, C. Gaber, C. Schluckner, M. Eichhorn-Gruber, G. Schwabegger, C. Hochenauer, Development of a numerically efficient approach based on coupled CFD / FEM analysis for virtual fire resistance tests—Part B: Deformation process of a steel structure, Fire Mater. 44 (2020) 704–723, http://dx.doi.org/10.1002/fam.2846.

[29] J.A. Feenstra, H. Hofmeyer, R. van Herpen, M. Mahendran, Automated two-way coupling of CFD fire simulations to thermomechanical FE analyses at the overall structural level, Fire Saf. J. 96 (2018) 165–175, http://dx.doi.org/10.1016/j.firesaf.2017.11.007.

[30] R. Prieler, S. Pletzer, S. Thumser, G. Schwabegger, C. Hochenauer, Numerical simulation of a fire resistance test and prediction of the flue gas leakage using CFD/FEM coupling, in: Applications of Structural Fire Engineering, Ljubljana, Slovenia, 2021, pp. 382–387.
[31] R. Prieler, B. Ortner, S. Thumser, G. Schwabegger, C. Hochenauer, Wall deformation during fire resistance tests - A comparative study between hollow-brick walls and gypsum-sheathed stud walls, in: Applications of Structural Fire Engineering, Ljubljana, Slovenia, 2021, pp. 137–142.
[32] R. Prieler, P. Kitzmüller, S. Thumser, G. Schwabegger, C. Hochenauer, Experimental analysis of the wall deformation of masonry brick and gypsum–sheathed stud walls during standardized fire resistance tests of steel doors, Fire Mater. 47 (2023) 305–321, http://dx.doi.org/10.1002/fam.3098.
[33] Y. Dias, M. Mahendran, K. Poologanathan, Full-scale fire resistance tests of steel and plasterboard sheathed web-stiffened stud walls, Thin-Walled Struct. 137 (2019) 81–93, http://dx.doi.org/10.1016/j.tws.2018.12.027.
[34] J. Pancheti, M. Mahendran, Fire resistance of external light gauge steel framed walls clad with autoclaved aerated concrete panels, Thin-Walled Struct. 167 (2021) 108201, http://dx.doi.org/10.1016/j.tws.2021.108201.
[35] S. Gnanachelvam, A. Ariyanayagam, M. Mahendran, Effects of insulation materials and their location on the fire resistance of LSF walls, J. Build. Eng. 44 (2021) 103323, http://dx.doi.org/10.1016/j.jobe.2021.103323.
[36] A.D. Ariyanayagam, M. Mahendran, Fire performance of load bearing LSF wall systems made of low strength steel studs, Thin-Walled Struct. 130 (2018) 487–504, http://dx.doi.org/10.1016/j.tws.2018.05.018.
[37] Y. Tao, M. Mahendran, A. Ariyanayagam, Numerical study of LSF walls made of cold-formed steel hollow section studs in fire, Thin-Walled Struct. 167 (2021) 108181, http://dx.doi.org/10.1016/j.tws.2021.108181.
[38] W. Chen, J. Jiang, J. Ye, Q. Zhao, K. Liu, C. Xu, Thermal behavior of external-insulated cold-formed steel non-load-bearing walls exposed to different fire conditions, Structures 25 (2020) 631–645, http://dx.doi.org/10.1016/j.istruc.2020.03.044.
[39] W. Chen, J. Ye, Q. Zhao, J. Jiang, Full-scale experiments of gypsum-sheathed cavity-insulated cold-formed steel walls under different fire conditions, J. Constr. Steel Res. 164 (2020) 105809, http://dx.doi.org/10.1016/j.jcsr.2019.105809.
[40] A.Y. Nassif, I. Yoshitake, A. Allam, Full-scale fire testing and numerical modelling of the transient thermo-mechanical behaviour of steel-stud gypsum board partition walls, Constr. Build. Mater. 59 (2014) 51–61, http://dx.doi.org/10.1016/j.conbuildmat.2014.02.027.
[41] J. Ye, W. Chen, Simplified calculation of fire resistant temperature for cold-formed steel load-bearing composite walls, Structures 28 (2020) 1661–1674, http://dx.doi.org/10.1016/j.istruc.2020.09.077.
[42] Y. Yu, P. Tian, M. Man, Z. Chen, L. Jiang, B. Wei, Experimental and numerical studies on the fire-resistance behaviors of critical walls and columns in modular steel buildings, J. Build. Eng. 44 (2021) 102964, http://dx.doi.org/10.1016/j.jobe.2021.102964.
[43] T. Abeysiriwardena, M. Mahendran, Numerical modelling and fire testing of gypsum plasterboard sheathed cold-formed steel walls, Thin-Walled Struct. 180 (2022) 109792, http://dx.doi.org/10.1016/j.tws.2022.109792.
[44] A.Y. Nassif, I. Yoshitake, V. Vimonsatit, Thermal and mechanical transient behaviour of steel doors installed in non-load-bearing partition wall assemblies during exposure to the standard fire test, Fire Mater. 40 (2016) 1070–1089, http://dx.doi.org/10.1002/fam.2365.
[45] R. Prieler, M. Mayrhofer, C. Gaber, H. Gerhardter, C. Schluckner, M. Landfahrer, M. Eichhorn-Gruber, G. Schwabegger, C. Hochenauer, CFD-based optimization of a transient heating process in a natural gas fired furnace using neural networks and genetic algorithms, Appl. Therm. Eng. 138 (2018) 217–234, http://dx.doi.org/10.1016/j.applthermaleng.2018.03.042.
[46] BS EN1993-1-2. Eurocode 3: Design of steel structures - Part 1-2: General rules - Structural fire design.
[47] W. Luecke, S. Banovic, D. McColskey, High-Temperature Tensile Constitutive Data and Models for Structural Steels in Fire: NIST Technical Note 1714, National Institute of Standards and Technology, 2011.
[48] R. Prieler, P. Kitzmüller, S. Thumser, G. Schwabegger, E. Kaschnitz, C. Hochenauer, Experimental analysis of moisture transfer and phase change in porous insulation exposed to fire and its effect on heat transfer, Int. J. Heat Mass Transfer 160 (2020) 120207, http://dx.doi.org/10.1016/j.ijheatmasstransfer.2020.120207.
[49] B. Weber, Heat transfer mechanisms and models for a gypsum board exposed to fire, Int. J. Heat Mass Transfer 55 (2012) 1661–1678, http://dx.doi.org/10.1016/j.ijheatmasstransfer.2011.11.022.
[50] R. Prieler, R. Langbauer, H. Gerhardter, P. Kitzmüller, S. Thumser, G. Schwabegger, C. Hochenauer, Modelling approach to predict the fire-related heat transfer in porous gypsum based on multi-phase simulations including water vapour transport, phase change and radiative heat transfer, Appl. Therm. Eng. 206 (2022) 118013, http://dx.doi.org/10.1016/j.applthermaleng.2021.118013.
[51] ANSYS Inc., ANSYS Fluent Theory Guide, ANSYS Inc., Canonsburg, PA, US, 2018.
[52] W. Ranz, W. Marshall, Evaporation from drops, part I and part II, Chem. Eng. Prog. 48 (1952) 173–180.
[53] W. Ranz, W. Marshall, Evaporation from drops, part I, Chem. Eng. Prog. 48 (1952) 141–146.
[54] J. Richter, K. Staněk, Measurements of water vapour permeability – Tightness of fibreglass cups and different sealants and comparison of μ-value of gypsum plaster boards, Procedia Eng. 151 (2016) 277–283, http://dx.doi.org/10.1016/j.proeng.2016.07.377.
[55] W. Lee, A Pressure Iteration Scheme for Two-Phase Modeling: Technical Report LA-UR 79-975, Los Alamos Scientific Laboratory, Los Alamos, NM, US, 1979.
[56] A. Loeb, Thermal conductivity: VIII, A theory of thermal conductivity of porous materials, J. Am. Ceram. Soc. 37 (1954) 96–99.
[57] D.P. Bentz, K.R. Prasad, J.C. Yang, Towards a methodology for the characterization of fire resistive materials with respect to thermal performance models, Fire Mater. 30 (2006) 311–321, http://dx.doi.org/10.1002/fam.916.
[58] C.T. Do, D.P. Bentz, P.E. Stutzman, Microstructure and thermal conductivity of hydrated calcium silicate board materials, J. Build. Phys. 31 (1) (2007) 55–67, http://dx.doi.org/10.1177/1744259107079020.
[59] K. Ghazi Wakili, M. Koebel, T. Glaettli, M. Hofer, Thermal conductivity of gypsum boards beyond dehydration temperature, Fire Mater. 39 (2015) 85–94, http://dx.doi.org/10.1002/fam.2234.
[60] ANSYS Inc., ANSYS Mechanical User Guide, ANSYS Inc., Canonsburg, PA, US, 2018.
[61] J.C. Simo, T.A. Laursen, An augmented Lagrangian treatment of contact problems involving friction, Comput. Struct. 42 (1992) 97–116.
[62] R. Prieler, B. Klemm, S. Pletzer, S. Thumser, G. Schwabegger, C. Hochenauer, Pressure increase in enclosures of steel doors and its effect on the deformation process during fire resistance tests - A numerical study, in: Applications of Structural Fire Engineering, Ljubljana, Slovenia, 2021, pp. 174–179.